Theoretical Investigations on Two-Dimensional Optical Ion Trapping

by

Zewen Sun

A thesis
presented to the University of Waterloo
in fulfillment of the
thesis requirement for the degree of
Master of Science
in
Physics (Quantum Information)

Waterloo, Ontario, Canada, 2022

Author's Declaration

I hereby declare that I am the sole author of this thesis. This is a true copy of the thesis, including any required final revisions, as accepted by my examiners.

I understand that my thesis may be made electronically available to the public.

Abstract

Trapped ion systems have become one of the important platforms for quantum information processing (QIP) experiments. However, conventional Paul ion traps suffer from micromotion effect, which makes it difficult to extend the trapped ion crystals beyond one-dimensional (1D) linear chain configuration, and limits the versatility of the systems. In this thesis, we propose a scheme of trapping two-dimensional (2D) ion crystals by combining conventional and optical trapping techniques. Integrating an optical cavity into linear Paul ion trap allows us to introduce an optical trapping period during which quantum gates can be performed without micromotion effect. We explored the required trapping parameters to constraining the system in 2D structure, by numerically calculating the equilibrium positions of ions under the potential defined by all trapping parameters. We then study the stability of 2D ion crystals between different spatial configurations, which do not arise from 1D systems. We also provide estimation of trapping lifetime by estimating heating rate of the system contributed from different sources which cannot be avoided by improving experimental designs. We find it is possible to trap tens of Yb^+ ions optically with our scheme for a potentially long enough lifetime to perform QIP experiments, followed with the discussion on how to scale up the system. Strategies for trapping parameters optimization can be developed based on our stability analysis such that the optical cavity trap can be designed and built to fit different QIP experiments with experimentally feasible parameters.

Acknowledgements

I want to thank Dr. Kazi Rajibul Islam for his support and supervision during my MSc. program. His leadership and research skills made it possible for me develop myself in a well organized group.

I would like to thank Yi Hong Teoh. His "Trapped Ion Calculator" Python package provides enormous convenience for the coding works involved in this thesis.

I would like to thank Dr. Fereshteh Rajabi for the consistency check on AC Stark shift calculations of hyperfine levels of $^{171}Yb^{+}$ ions, which is an important portion of this work.

I must express my gratitude to all my colleagues in quantum information with trapped ions (QITI) group for their generous help, enlightenment, and discussions.

Dedication

This is dedicated to every reader.

Table of Contents

List of Figures

List of Tables

Chapter 1

Introduction

The discovery of quantum mechanics was regarded as one of the starting signs of modern physics, and its development has provided fundamental theoretical support for an numerous of modern technologies. Although quantum mechanics is a well developed theory with rich applications, it is still very difficult to solve many-body interacting systems with quantum mechanics. Since in quantum mechanics, interacting systems are described by nonlinear partial differential equations, which do not have analytic solutions in general. Numerical calculation is the only way to solve it, but the computational complexity scales up exponentially with the number of particles involved in the systems, e.g. the Hilbert space of N number of two-level systems has dimension of 2^N. Our progress of understanding the physical world is eventually limited by our computing capability.

Quantum computation provides a solution to the problem of insufficient computing capability, since by converting classical bits to quantum bits, one quantum algorithms can be performed much faster than classical algorithms. In addition, instead of calculating the exact solution, we can simulate many-body interacting systems and measure how it evolve in time. Ions are good candidates to simulate interacting systems due to their strong Coulomb interactions. The strong Coulomb interactions can also be used to create quantum logic gates, which relate to quantum computation. These are part of the reasons which motivate the idea of quantum simulation and computation with trapped ion systems. Quantum computation and simulation are two branches of quantum information. In this chapter, we will introduce trapped ion system as a platform for quantum information processing (QIP) experiments.

1.1 Tapped-ion Platform

Due to the phonon-mediated strong spin-spin interactions, the clean trapping environment, and convenient spin dependent measurement capacity, trapped ion systems have become one of the leading platforms to perform QIP experiments. With each ion presented as a quantum bit (qubit), the two qubit states are encoded in the long-lived ground internal hyperfine energy states. The two qubit states $|0\rangle$ and $|1\rangle$, sometimes also called as spin states $|\uparrow\rangle$ and $|\downarrow\rangle$, can be coupled using two Raman beams or microwaves driving the two-photon transition, allowing arbitrary single-qubit rotation. The feasibility of constructing quantum computers with trapped ion systems was demonstrated by the first scheme to implement controlled NOT gate [1], and more robust schemes [2, 3] are proposed later. A universal set of quantum gates can be constructed by a sequence of single qubit rotations and controlled NOT gates [4]. The ions can be trapped with conventional traps, such as Paul trap and Penning trap, or conventional and optical combined hybrid traps.

Paul ion trap [5] uses a combination of static (DC) and oscillating (AC) electric fields to trap ions, since charged particles cannot be trapped solely be static electric field(s), stated by Earnshaw's theorem. The DC field creates confinement to ions at one direction, while the AC field creates both confinement and anti-confinement at the other two directions. The confining and anti-confining direction is changing over time at a faster rate compared to time for the ions to escape the trap, therefore the AC field creates an time averaged trapping pseudo-potential for ions. The AC electric field oscillates at radio frequency (RF) and it is also called RF field. If a single ion is trapped inside the Paul trap, and the ion is not perfectly located at center of the potential, the oscillating field will continuously raise and lower the potential energy of the ion, causing the ion to move. The motion is predicted by Mathieu equation, which can be solved numerically. This motion can excite unwanted normal modes of the system, which is the so-called micromotion problem of Paul trap.

The trapped ions can form a one-dimensional (1D) linear chain configuration, or a two-dimensional (2D) plane configuration [6], and the later one with enriched phase diagrams opens up a new realm for quantum simulation of many-body systems. There exist some problems that are native to the 2D and 3D structure of the model which cannot be studied with 1D systems, e.g. geometrical magnetic frustration, making 2D trapped ion systems to be intrinsic different from 1D linear chain of trapped ions. However, the micromotion problem poses challenges to extending the system beyond 1D, since the further the ion is located from the center the stronger micromotion effect it will suffer.

Replacing the AC electric potential by optical potential is one of the approaches to eliminate the micromotion effect, but it introduce other problems to the trap. Optical

ion trap experiments have been performed on a system of one $^{138}Ba^{+}$ ion [7, 8], and a system of up to 6 $^{138}Ba^{+}$ ions in a linear chain [9], using a global Gaussian beam. Optical trap depth is normally many orders of magnitude smaller than conventional trap depth, and this is one of the reasons making optical trapping lifetime to be much shorter than conventional trapping. Ions in strong light fields also scatter photons, and the scattering rate is proportional to laser intensity. The scattering events can destroy coherence of the quantum states of the ions, heat up the temperature of the system, as well as potentially send the ions to some unwanted internal states. In this work, we theoretically investigate the feasibility of trapping ions in 2D structure using optical trapping techniques, in order to simulate 2D spin systems. We provide quantitative estimation of the different adverse effects of optical trapping to determine whether QIP experiments can be performed with our 2D trapped ion system.

1.2 Thesis Outline

In Chapter 1, we introduce QIP with trapped ion platform and the possibility of integrating optical trapping techniques into conventional ion traps. We will explore how ions can be trapped using lasers, find out the trapping parameters, and analyze the stability of the system:

1. Chapter 2: We introduce the basic concepts and mechanisms of optical trapping, including AC Stark shift, Rabi frequency, and scattering rate. We start the introduction with a simple two-level system, and then extend it to more complicated systems, i.e. ions. Finally, using the knowledge we obtained, we explore the optical properties of ion species for trapping.

2. Chapter 3: We introduce optical cavity and our optical cavity setup, along with all the trapping parameters characterizing the trap. We then find the required trapping parameters for 2D trapping, by studying the properties of 2D ion crystals.

3. Chapter 4: Since the equilibrium positions of trapped 2D ion crystals are not unique, we investigate the potential barrier between different equilibrium positions to study their stability in optical cavity trap. Next, we estimate trapping lifetime and heating rate, by considering different sources of heating.

Chapter 2

Optical Dipole Trap for Ions

From a classical mechanics point of view, when a laser beam shine on an atom or ion, the electric field from this laser can polarize the atom or ion into an electric dipole. This dipole in will experience a potential given by the electric field, and using this potential to trap atom(s) or ion(s) leads to the idea of optical dipole trap. The atom or ion feels a potential since the alternating electric field at its position shifts its internal energy levels, and this energy shift is called AC Stark shift. Therefore, understanding AC Stark shift is the first step to understand optical dipole trap. For ions in light field, they have a chance to scatter a photon, and this scattering event will decay from an excited state to a lower energy state. Scattering events can change the value of AC Stark shift, heat up the ion, as well as break coherence of the quantum state, which undermines trapping stability and create errors in QIP experiments. Thus, for optical dipole trap, we wish to have high AC Stark shift, and small scattering rate.

In this chapter, we first study AC Stark shift and scattering rate. Next, we find out how much trap frequency can a typical Gaussian beam optical dipole trap provide. Then, we discuss the analytic model estimating single ion optical trapping lifetime. Finally, we search for ion species on the periodic table to determine what ions are good candidate for optical trapping based on their optical properties.

2.1 AC Stark Shift

The classical interpretation provides a good way to intuitively understand AC Stark Shift, but we will start from quantum mechanics point of view to derive an expression for AC

Stark Shift in terms of Rabi frequency and laser detuning, where Rabi frequency is a parameter can be obtained from experimental measurements, and laser detuning is the angular frequency different between laser and atomic transition.

In this section, we first derive AC Stark shift for a two-level-system. This AC Stark shift depends on Rabi frequency, so we then derive the relation between Rabi frequency and Einstein A coefficient. Next, we extend this two-level AC Stark shift calculation to ions with multiple levels and hyperfine splitting. AC Stark shift calculations will provide guidance to us in designing optical cavity trap and analyzing stability of trapped ion system, in later chapters.

2.1.1 AC Stark Shift for a Two-Level System

A two-level system can be viewed as an imaginary atom with only two internal states. We will call the two internal states as ground state $|g\rangle$ and excited state $|e\rangle$. Once this two-level system, considering it as a hydrogen atom, is placed inside a time varying electric field, e.g. a laser, the electric field creates a additional potential energy $V_e(\vec{r},t) = -e\vec{E}(\vec{r},t)\cdot\vec{r}$, where $\vec{r}$ is the vector from nucleus to its electron, hence the atomic-field interaction Hamiltonian is

$$H' = -e\vec{E}(\vec{r},t)\cdot\vec{r}, \tag{2.1}$$

with

$$\vec{E}(\vec{r},t) = E_0\cos(\omega_l t)\hat{\epsilon}, \tag{2.2}$$

where ω_l is angular frequency of the laser. Now the total Hamiltonian is the sum of atomic Hamiltonian H_a and H' ,

$$H = H_a + H'. \tag{2.3}$$

AC Stark shift of this system is the shift of eigenenergies from H_a to H due to the presence of H'. To do this, we define a basis as ordered set $\alpha = \{|\phi_1\rangle = |g\rangle, |\phi_2\rangle = |e\rangle\}$, where $|\phi_i\rangle$ are time independent energy eigenstates of H_a, and the time dependent energy eigenstates are $|\phi_i(t)\rangle = e^{-iHt/\hbar}|\phi_i\rangle$, then the matrix elements of H' are

$$H'_{ij} = \langle\phi_i(t)|\, H' \,|\phi_j(t)\rangle = -eE_0\cos(\omega_l t)\,\langle\phi_i(t)|\,\hat{\epsilon}\cdot\vec{r}\,|\phi_j(t)\rangle\,. \tag{2.4}$$

We will show all diagonal elements of H' are zero, by using a theorem stated as, if potential energy $V(\vec{r})$ has the property of $V(\vec{r}) = V(-\vec{r})$, the wavefunction of energy eigenstates, in coordinate representation, have defined parity.

For this hydrogen atom, the electron experience a potential of $V(\vec{r}) = -e^2/4\pi\epsilon_0|\vec{r}| = V(-\vec{r})$, and ϕ_i are eigenenergies of H_a, so ϕ_i has defined parity at any time. No matter

even or odd, $|\phi_i|^2$ is an even function, and $\hat{\epsilon}\cdot\vec{r}|\phi_i|^2$ is odd, thus once it is integrated over all space, we have

$$\begin{aligned} H'_{ii} &= -eE_0\cos(\omega_l t)\,\langle\phi_i(t)|\,\vec{r}\,|\phi_i(t)\rangle \\ &= -eE_0\cos(\omega_l t)\int_{\text{all space}}\hat{\epsilon}\cdot\vec{r}\;\phi_i^*(\vec{r},t)\phi_i(\vec{r},t)\;dV \\ &= -e\vec{E}(\vec{r},t)\cdot\int_{\text{all space}}\hat{\epsilon}\cdot\vec{r}\;|\phi_i(\vec{r},t)|^2\;dV \\ &= 0, \end{aligned}$$

i.e. all diagonal elements of H' are zero.

Since we choose the basis as eigenbasis of H_a, H_a is a diagonal matrix, and all off-diagonal elements are zero. Now we know H_a has only diagonal elements, and H' has only off-diagonal elements, so we have

$$H_{ii} = (H_a)_{ii}, \tag{2.5}$$

and for $i \neq j$

$$\begin{aligned} H_{ij} &= H'_{ij} \\ &= \langle\phi_i(t)|\,H'\,|\phi_j(t)\rangle \\ &= -eE_0\cos(\omega_l t)\,\langle\phi_i(t)|\,\hat{\epsilon}\cdot\vec{r}\,|\phi_j(t)\rangle\,. \end{aligned}$$

Define

$$\Omega_{ij} \equiv -\frac{eE_0}{\hbar}\,\langle\phi_i(t)|\,\hat{\epsilon}\cdot\vec{r}\,|\phi_j(t)\rangle\,, \tag{2.6}$$

such that we can write

$$H_{ij} = H'_{ij} = \hbar\Omega_{ij}\cos(\omega_l t) = \frac{\hbar\Omega_{ij}}{2}(e^{i\omega_l t} + e^{-i\omega_l t}). \tag{2.7}$$

Note that Ω_{ij} can be a complex number. Its magnitude is called Rabi frequency Ω

$$\Omega \equiv \sqrt{|\Omega_{ij}|^2} = \sqrt{|\Omega_{ji}|^2} = \sqrt{\Omega_{ij}\Omega_{ji}}. \tag{2.8}$$

This H is time dependent. We will transform H into a rotating reference frame, then use an approximation to make it time independent. The unitary matrix which transform H into the rotating reference frame is time dependent, so we define it as $U(t)$, and let $|\tilde{\Psi}\rangle$ be the state in the rotating reference frame after the transform, we have

$$|\tilde{\Psi}\rangle = U(t)\,|\Psi\rangle\,, \tag{2.9}$$

$$H\left|\Psi\right\rangle = i\hbar\frac{\partial|\Psi\rangle}{\partial t}. \tag{2.10}$$

We want to find a effective Hamiltonian in the rotating reference frame which satisfy

$$H_{\text{eff}}|\tilde{\Psi}\rangle = i\hbar\frac{\partial|\tilde{\Psi}\rangle}{\partial t} \tag{2.11}$$

If we can find such H_{eff}, AC Stark shift can be obtained by diagonalizing H_{eff}. Note that $U(t)$ does not necessarily commute with H or time evolution operator. By using Eq. (2.9) and (2.10), we have

$$\begin{aligned}
\frac{\partial|\tilde{\Psi}\rangle}{\partial t} &= \frac{\partial\big(U(t)\left|\Psi\right\rangle\big)}{\partial t} \\
&= \dot{U}(t)\left|\Psi\right\rangle + U(t)\frac{\partial|\Psi\rangle}{\partial t} \\
&= \dot{U}(t)\left|\Psi\right\rangle - \frac{i}{\hbar}U(t)H\left|\Psi\right\rangle \\
&= \dot{U}(t)\Big(U^{\dagger}(t)U(t)\Big)\left|\Psi\right\rangle - \frac{i}{\hbar}U(t)H\Big(U^{\dagger}(t)U(t)\Big)\left|\Psi\right\rangle \\
&= \Big(\dot{U}(t)U^{\dagger}(t) - \frac{i}{\hbar}U(t)HU^{\dagger}(t)\Big)U(t)\left|\Psi\right\rangle \\
&= \Big(\dot{U}(t)U^{\dagger}(t) - \frac{i}{\hbar}U(t)HU^{\dagger}(t)\Big)\left|\tilde{\Psi}\right\rangle.
\end{aligned}$$

Multiply both sides by $i\hbar$, we have

$$\begin{aligned}
i\hbar\frac{\partial|\tilde{\Psi}\rangle}{\partial t} &= i\hbar\Big(\dot{U}(t)U^{\dagger}(t) - \frac{i}{\hbar}U(t)HU^{\dagger}(t)\Big)\left|\tilde{\Psi}\right\rangle \\
&= \Big(i\hbar\ \dot{U}(t)U^{\dagger}(t) + U(t)HU^{\dagger}(t)\Big)\left|\tilde{\Psi}\right\rangle \\
&= H_{\text{eff}}\left|\tilde{\Psi}\right\rangle.
\end{aligned}$$

Overall, the effective Hamiltonian in the rotating reference frame is

$$H_{\text{eff}} = i\hbar\ \dot{U}(t)U^{\dagger}(t) + U(t)HU^{\dagger}(t). \tag{2.12}$$

If we define H_a as

$$H_a = \frac{\hbar}{2}\begin{bmatrix} -\omega_a & 0 \\ 0 & \omega_a \end{bmatrix}. \tag{2.13}$$

In other words, we defining the energy difference of energy eigenstates $|g\rangle$ and $|e\rangle$ to be $\hbar\omega_a$, where ω_a is atomic resonance frequency. Combining Eq. (2.13) and (2.7), the total Hamiltonian is

$$H = H_a + H' \tag{2.14}$$

$$= \frac{\hbar}{2}\begin{bmatrix} -\omega_a & \Omega_{12}(e^{i\omega_l t} + e^{-i\omega_l t}) \\ \Omega_{21}(e^{i\omega_l t} + e^{-i\omega_l t}) & \omega_a \end{bmatrix}. \tag{2.15}$$

The time dependent unitary matrix $U(t)$ that transform H into H_{eff} is

$$U(t) = \begin{bmatrix} e^{-i\omega_l t/2} & 0 \\ 0 & e^{i\omega_l t/2} \end{bmatrix}. \tag{2.16}$$

Then we have

$$i\hbar\, \dot{U}(t)U^\dagger(t) = i\hbar \begin{bmatrix} -\frac{i\omega_l}{2}e^{-i\omega_l t/2} & 0 \\ 0 & \frac{i\omega_l}{2}e^{i\omega_l t/2} \end{bmatrix} \begin{bmatrix} e^{i\omega_l t/2} & 0 \\ 0 & e^{-i\omega_l t/2} \end{bmatrix} \tag{2.17}$$

$$= \frac{\hbar}{2}\begin{bmatrix} \omega_l & 0 \\ 0 & -\omega_l \end{bmatrix}, \tag{2.18}$$

and

$$U(t)HU^\dagger(t)$$

$$= \frac{\hbar}{2}\begin{bmatrix} e^{-i\omega_l t/2} & 0 \\ 0 & e^{i\omega_l t/2} \end{bmatrix} \begin{bmatrix} -\omega_a & \Omega_{12}(e^{i\omega_l t} + e^{-i\omega_l t}) \\ \Omega_{21}(e^{i\omega_l t} + e^{-i\omega_l t}) & \omega_a \end{bmatrix} \begin{bmatrix} e^{i\omega_l t/2} & 0 \\ 0 & e^{-i\omega_l t/2} \end{bmatrix} \tag{2.19}$$

$$= \frac{\hbar}{2}\begin{bmatrix} -\omega_a & \Omega_{12}e^{-i2\omega_l t} \\ \Omega_{21}e^{i2\omega_l t} & \omega_a \end{bmatrix}. \tag{2.20}$$

Define laser detuning as $\delta \equiv \omega_l - \omega_a$. For the case $\delta \ll (\omega_l + \omega_a) \approx 2\omega_l$, neglect the terms $e^{i(\omega_l+\omega_a)t}$ compared to the ones of order $e^{i\delta t}$. This approximation is called rotating wave approximation, which allows us to write

$$U(t)HU^\dagger(t) = \frac{\hbar}{2}\begin{bmatrix} -\omega_a & \Omega_{12} \\ \Omega_{21} & \omega_a \end{bmatrix} \tag{2.21}$$

Substitute Eq. (2.18) and (2.20) into Eq. (2.12), we have

$$H_{\text{eff}} = i\hbar\, \dot{U}(t)U^\dagger(t) + U(t)HU^\dagger(t) \tag{2.22}$$

$$= \frac{\hbar}{2}\begin{bmatrix} \delta & \Omega_{12} \\ \Omega_{21} & -\delta \end{bmatrix}. \tag{2.23}$$

This matrix has eigenvalues of

$$\begin{aligned}\lambda &= \pm\frac{\hbar}{2}\sqrt{\delta^2+\Omega^2} \\ &= \pm\frac{\hbar}{2}\delta\sqrt{1+\frac{\Omega^2}{\delta^2}},\end{aligned}$$

where we use Rabi frequency square Ω^2 to replace $\Omega_{12}\Omega_{21}$. In the limit where $\Omega \ll |\delta|$, by using binomial expansion, we have

$$\lambda = \pm\frac{\hbar}{2}\delta(1+\frac{\Omega^2}{2\delta^2}). \tag{2.24}$$

Hence, within the rotating reference frame, AC Stark shift of the two levels are

$$\Delta E_g = \frac{\hbar\Omega^2}{4\delta},\ \Delta E_e = -\frac{\hbar\Omega^2}{4\delta}. \tag{2.25}$$

This is the results calculated from a small detuning case, $\delta \ll \omega_l$, for which rotating wave approximation applies, and Rabi frequency much smaller than detuning, $\Omega \ll |\delta|$, which is always true in the situations where we are interested in.

As for the larger laser detuning case, where rotating wave approximation is not valid, AC Stark shift calculation is discussed in [10], and ground state AC Stark shift is given by

$$\Delta E_g = -\frac{3\pi c^2}{2\omega_a^3}\left(\frac{A}{\omega_a-\omega_l}+\frac{A}{\omega_a+\omega_l}\right)\ I \tag{2.26}$$

where A is Einstein A coefficient of transition from $|e\rangle$ and $|g\rangle$. This result is valid when excited state does not get strongly populated, in other words, when intensity of diving field is not too high, or detuning is not too small.

To understand how the system evolve in time, we need to solve for the energy eigenstates of Eq. (2.23), where we have

$$|\Psi_+\rangle = \frac{\left(\delta+\sqrt{\delta^2+\Omega^2}\right)|g\rangle}{\Omega\sqrt{1+\frac{\left(\delta+\sqrt{\delta^2+\Omega^2}\right)^2}{\Omega^2}}}+\frac{|e\rangle}{\sqrt{1+\frac{\left(\delta+\sqrt{\delta^2+\Omega^2}\right)^2}{\Omega^2}}}, \tag{2.27}$$

$$|\Psi_-\rangle = \frac{\left(\delta-\sqrt{\delta^2+\Omega^2}\right)|g\rangle}{\Omega\sqrt{1+\frac{\left(\delta-\sqrt{\delta^2+\Omega^2}\right)^2}{\Omega^2}}}+\frac{|e\rangle}{\sqrt{1+\frac{\left(\delta-\sqrt{\delta^2+\Omega^2}\right)^2}{\Omega^2}}}. \tag{2.28}$$

Recall that $\{|g\rangle, |e\rangle\}$ is the eigenbasis for H_a, and here $|\Psi_+\rangle$ and $|\Psi_-\rangle$ are eigenstates of H_{eff}. By taking $\Omega \ll |\delta|$, we can approximate them as

$$|\Psi_+\rangle = \frac{\left(\frac{2\delta}{\Omega} + \frac{\Omega}{2\delta}\right)|g\rangle}{\sqrt{1 + \left(\frac{2\delta}{\Omega} + \frac{\Omega}{2\delta}\right)^2}} + \frac{|e\rangle}{\sqrt{1 + \left(\frac{2\delta}{\Omega} + \frac{\Omega}{2\delta}\right)^2}}, \tag{2.29}$$

$$|\Psi_-\rangle = \frac{(\Omega/2\delta^2)|g\rangle}{\sqrt{1 + \frac{\Omega^2}{4\delta^4}}} + \frac{|e\rangle}{\sqrt{1 + \frac{\Omega^2}{4\delta^4}}}. \tag{2.30}$$

If the system is initially at $|g\rangle$, and we want to know how this system evolve in time, Eq. (2.29) and (2.30) give us the relation between $\{|g\rangle, |e\rangle\}$ and $\{|\Psi_+\rangle, |\Psi_-\rangle\}$. We can use it to find the unitary matrix that transform the time evolution operator from energy eigenbasis to $\{|g\rangle, |e\rangle\}$ basis, and the probability of the system being in $|e\rangle$ state if it is initially at $|g\rangle$ is

$$P(e|g) = \left|\frac{1}{\sqrt{1 + \frac{\Omega^2}{4\delta^4}}} \frac{1}{\sqrt{1 + \left(\frac{2\delta}{\Omega} + \frac{\Omega}{2\delta}\right)^2}}\right|^2 \cdot \left|-e^{-i\frac{\sqrt{\delta^2+\Omega^2}}{2}t} + e^{i\frac{\sqrt{\delta^2+\Omega^2}}{2}t}\right|^2 \tag{2.31}$$

$$= \left(\frac{1}{\frac{4\delta^2}{\Omega^2} + 4 + \frac{\Omega^2}{\delta^2} + \frac{\Omega^4}{16\delta^4}}\right) 4\sin^2\left(\frac{\sqrt{\delta^2+\Omega^2}}{2}t\right) \tag{2.32}$$

$$= \left(\frac{\Omega^2}{\delta^2+\Omega^2}\right) \sin^2\left(\frac{\sqrt{\delta^2+\Omega^2}}{2}t\right). \tag{2.33}$$

Some terms was omitted in Eq. (2.32) due to $\Omega \ll |\delta|$ assumption. This probability is a sinusoidal function with amplitude $\frac{\Omega^2}{\delta^2+\Omega^2}$ and angular frequency $\sqrt{\delta^2+\Omega^2}$.

2.1.2 Rabi Frequency

In last section, we have expressed AC Stark shift of a two-level system in terms of laser detuning and Rabi frequenc, but the magnitude of Rabi frequency is still unknown. In this section, we will derive an expression for Rabi frequency, which shows Rabi frequency is related to Einstein A coefficient, atomic transition wavelength, and laser intensity. Einstein A coefficients for specific transitions can be retrieved from NIST atomic spectra database.

Let $|i\rangle$ be ground state, and $|k\rangle$ be excited state. I'm following the notation used on NIST atomic spectra database. An excited atom in state $|k\rangle$ can decay back to state $|i\rangle$

spontaneously without an external radiation field. This process is spontaneous emission. The probability of such a spontaneous emission per second is

$$\frac{d\mathcal{P}_{ki}^{\text{sp. em.}}}{dt} \equiv A_{ki},$$

where A_{ki} is Einstein A coefficient, and it is a parameter solely depends on the wave function of state $|k\rangle$ and $|i\rangle$.

A classical oscillating electric dipole with electric dipole moment

$$\vec{p}(t) = q\vec{d} = \vec{p}_0 \sin(\omega t)$$

radiates total average power of

$$\langle P \rangle = \frac{\langle p^2 \rangle \omega^4}{6\pi\epsilon_0 c^3}. \tag{2.34}$$

For an atom emits a photon by transition from $|k\rangle$ to $|i\rangle$, the transition dipole moment $\vec{\mu}_{ki} = \langle \vec{p} \rangle$ is defined as

$$\vec{\mu}_{ki} \equiv e \langle k | \vec{r} | i \rangle . \tag{2.35}$$

By evaluating the integration of wavefunction of hydrogen-like atom, we have relation

$$\langle p^2 \rangle = 2|\vec{\mu}_{ki}|^2. \tag{2.36}$$

For a single atom emits a photon by transition from $|k\rangle$ to $|i\rangle$, Einstein A coefficient is related to $\langle P \rangle$ by

$$\langle P \rangle = A_{ki} \hbar \omega_a, \tag{2.37}$$

where $\hbar\omega_a$ is the energy difference between the two states. From (2.34), (2.36), and (2.37) we have

$$A_{ki} = \frac{\omega_a^3}{3\pi\epsilon_0 \hbar c^3} \, |\vec{\mu}_{ki}|^2. \tag{2.38}$$

Recall Rabi frequency of two states $|k\rangle$ and $|i\rangle$ is defined as

$$\Omega \equiv -\frac{eE_0}{\hbar} |\langle k | \hat{\epsilon} \cdot \vec{r} | i \rangle|. \tag{2.39}$$

Define μ as $\hat{\epsilon} \cdot \vec{\mu}_{ki}$

$$\mu \equiv \hat{\epsilon} \cdot \vec{\mu}_{ki} = e \langle k | \hat{\epsilon} \cdot \vec{r} | i \rangle , \tag{2.40}$$

where μ is also referred as transition matrix element. We finally have

$$\mu = \sqrt{A_{ki} \frac{3\epsilon_0 \hbar \lambda_a^3}{8\pi^2}}. \tag{2.41}$$

Since $E_0 = \sqrt{2I/(\epsilon_0 c)}$, we have

$$\Omega = -\sqrt{A_{ki}\frac{3\lambda_a^3 I}{4\hbar\pi^2 c}}, \tag{2.42}$$

where λ_a is the atomic transition wavelength between the two states, and I is the intensity of the laser or light field. Sometimes the minus sign is ignored, since AC Stark shift is related to Ω^2.

2.1.3 AC Stark Shift for Ions

The internal states of ions, or more generally atoms, are not single particle states, in general. However, we will only consider alkali-like ions, and treat their internal states as single particle states. Alkali-like ions are referring to the ions with closed inner shell(s) and one outer valence electron. A shell is closed when it contains the maximum number of electrons permitted by Pauli exclusion principle. If all inner shells are closed, the electrons in those shells form $^1S_0$ state, where $^1S_0$ is using Russell-Saunders notation, $^{(2S+1)}L_J$. In this case, the state of out electron in Russell-Saunders notation can fully specify the electronic configuration of the ion, therefore we use the state of outer electron to represent the state of the ion.

Ions are not simple two-level systems, and their internal states consist of multiple states. However, ions under a laser field with specific wavelength can be treated as an ensemble of multiple two-level systems, since only specific two-level transitions can be excited by the laser field. For example, as for Ba^+, transition from ground $S_{1/2}$ state to $P_{1/2}$ has wavelength of 493.4 nm, and transition from $S_{1/2}$ state to $P_{3/2}$ has wavelength of 455.4 nm. If a Ba^+ ion is placed under 474 nm laser, the laser has the potential of exciting both $P_{1/2}$ and $P_{3/2}$ state, but once the Ba^+ reach $P_{1/2}$ state, it is very unlikely for such laser to excite the Ba^+ to $P_{3/2}$ state. Since the energy difference between $P_{1/2}$ and $P_{3/2}$ states is much smaller than the energy of a single photon from the laser. Therefore, AC Stark shift of ground $S_{1/2}$ state in this 3-level system, can be approximated as sum of AC Stark shift of $S_{1/2} \to P_{1/2}$ and $S_{1/2} \to P_{3/2}$ transitions. We can write it as

$$\Delta E_g = \sum_e \Delta E_e, \tag{2.43}$$

where ΔE_g is AC Stark shift of ground state, and ΔE_e refers to all excited states that are likely to be excited by the laser.

While saying $S_{1/2}$ state is the ground state of Ba^+, or more generally of all alkali-like ions, we have naively assumed all hyperfine states of $S_{1/2}$ state are degenerate. However, this is not true for any ion with nuclear spin quantum number $I \neq 0$. If we wish to know AC Stark shift of a particular hyperfine state of $S_{1/2}$ state, which could be more useful in trapped ion experiments, we need to apply Wigner–Eckart theorem, which states as

$$\langle F'\ m'_F|\, T^k_q\, |F\ m_F\rangle = \langle F\ k\ m_F\ q|F'\ m'_F\rangle\ \langle F'||T^k||F\rangle\,, \tag{2.44}$$

where T^k_q is the q-th component of the spherical tensor operator T^k of rank k, and $\langle F\ k\ m_F\ q|F'\ m'_F\rangle$ is the Clebsch–Gordan coefficient for coupling F with k to get F', and $\langle F'||T^k||F\rangle$ is some scalar that does not depend on m_F, m'_F, nor q, and is called reduced matrix element.

Since the operator for transition matrix element, $e\hat{\epsilon}\cdot\vec{r}$, is a spherical tensor operator of rank 1, we have

$$\langle F'\ m'_F|\, e\hat{\epsilon}_q\cdot\vec{r}\,|F\ m_F\rangle = \langle F\ 1\ m_F\ q|F'\ m'_F\rangle\ \langle F'||er||F\rangle\,, \tag{2.45}$$

where $q = -1, 0, +1$ represents σ^-, π, σ^+ polarized light, and primed variables refer to the excited states and the unprimed variables refer to the ground states. By introducing Wigner 3-j and 6-j symbols, we have

$$\begin{aligned}
&\langle F'\ m'_F|\, e\hat{\epsilon}_q\cdot\vec{r}\,|F\ m_F\rangle \\
&= (-1)^{F-1+m'_F}\sqrt{2F'+1}\begin{pmatrix} F & 1 & F' \\ m_F & q & -m'_F\end{pmatrix}\ \langle F'||er||F\rangle
\end{aligned} \tag{2.46}$$

$$\begin{aligned}
&= (-1)^{2F+m'_F+J'+I}\sqrt{(2F'+1)(2F+1)(2J'+1)}\begin{Bmatrix} J' & J & 1 \\ F & F' & I\end{Bmatrix} \\
&\quad\cdot\begin{pmatrix} F & 1 & F' \\ m_F & q & -m'_F\end{pmatrix}\ \langle J'||er||J\rangle\,.
\end{aligned} \tag{2.47}$$

In the last line, we have written the reduced matrix element in J-basis, allowing us to find the relation between transition matrix elements $\mu_{J'\to J}$ and $\mu_{F'\to F}$, as well as Rabi frequency $\Omega_{J'\to J}$ and $\Omega_{F'\to F}$. With this relation, if we can calculation AC Stark shift with $\Omega_{J'\to J}$, we should also be able to calculate AC Stark shift for hyperfine states with $\Omega_{F'\to F}$.

Note that sometime $\langle F'||er||F\rangle$ is written as $\langle \alpha' F'||er||\alpha F\rangle$, where this α refers to any variable that the reduced matrix element depends on, e.g. α can be principal quantum number.

2.2 Scattering Rate

Scattering of photons from atoms or ions caused by spontaneous emission is induced by vacuum fluctuations, thus, this process and scattering rate are not explained by time evolution operator obtained from Hamiltonian. When on atom or ion emits a photon, it will transit from an excited state downwards to a state with lower energy, or to the ground state. This process will also take the atom from a pure state, if it was in pure state, to a mixture state. When a system turn into a mixture state from a pure state, not only some information is lost, but also the system lose its coherence, creating errors to QIP experiments. Therefore, for any QIP experiment with trapped ion systems, we wish to eliminate this scattering rate, or perform our experiments in a short time scale such that the probability for the trapped ions to scatter a photon is very low.

From a two-level system treatment, if the atom is initially at ground state, the scattering rate of the atom under a laser with small detuning, is given by [11]

$$r_{\text{sca.}} = \frac{\Omega^2 A}{A^2 + 2\Omega^2 + 4\delta^2}, \tag{2.48}$$

where A is Einstein A coefficient of the transition.

As for large detuning, the scattering rate is [10]

$$r_{\text{sca.}} = -\frac{3\pi c^2}{2\hbar\omega_a^3}\left(\frac{\omega_l}{\omega_a}\right)^3\left(\frac{A}{\omega_a - \omega_l} + \frac{A}{\omega_a + \omega_l}\right)^2 I. \tag{2.49}$$

With the help from Eq. (2.42), and by taking $\delta \gg \Omega$, $\delta \gg A_{eg}$, and $\omega_l/\omega_a = 1$, we can see that the two equations for small and large detuning are now the same.

If we initialize the atom in ground state, and place it into a laser field, the total scattering rate from a multilevel treatment is similarly to the multilevel treatment of AC Stark shift

$$r_{\text{total sca.}} = \sum_e r_{\text{sca.},e}, \tag{2.50}$$

where $r_{\text{sca.},e}$ refers to the scattering rate from all $|g\rangle \to |e\rangle \to |g\rangle$ transitions that are likely to be excited by the laser. However, the $|e\rangle \to |g\rangle$ transition does not necessarily bring the atom back to the initial state, as it can go to other states, including hyperfine states, with lower energy compared to $|e\rangle$, and at later times, the initial condition is not longer valid, such that the calculation is not longer correct.

Since we wish to have small scattering rate, the equations tell us to choose lasers with low intensity or with large detuning. However, we also want to have large AC Stark shift,

as discussed in the following chapter. Since scattering rate follows $r_{\text{sca.}} \propto 1/\delta^2$ and AC Stark shift obeys $\Delta E \propto 1/\delta$, for building optical ion trap, the best strategy is to use lasers with large detuning and high intensity, such that scattering rate is suppressed by $r_{\text{sca.}} \propto 1/\delta^2$ term, and large AC Stark shift is provided by $\Delta E \propto I$ term.

2.3 Optical Dipole Trap

Since AC Stark shift is proportional to the laser intensity, if one have a nonuniform intensity distribution in space, ions in such field will experience different potential at different position, and this potential can be made to be trapping potential, which leads to the idea of optical trapping of ions. However, optical trap depth is normally much smaller than conventional trap depth, where conventional trap depth can easily exceed eV, $1\ e\text{V} \approx 12000\ \text{K}\cdot k_B$, whereas optical trap depth is measure in unit of $\text{mK} \cdot k_B$. Optical ion trap experiments have been performed on a system of one $^{138}\text{Ba}^+$ ion [7, 8], and a system of up to 6 $^{138}\text{Ba}^+$ ions in a linear chain [9], using a global Gaussian beam. In this section, we will find the trap frequencies in all 3 directions provided by a Gaussian beam.

For a Gaussian beam propagating at $+z$ direction, its intensity distribution is given by

$$I(s,z) = I_0 \left(\frac{w_0}{w(z)}\right)^2 \exp\left(\frac{-2s^2}{w(z)^2}\right), \tag{2.51}$$

where

$$s^2 \equiv x^2 + y^2,$$

$$I_0 \equiv I(s=0, z=0) \text{ and } w_0 \equiv w(z=0),$$

$w(z)$ is beam radius, and $w_0 \equiv w(z=0)$ is beam waist. Please notice that w is different from angular frequency ω, and it is given by

$$w(z) = w_0 \sqrt{1 + \left(\frac{z}{z_R}\right)^2}, \tag{2.52}$$

where

$$z_R = \frac{\pi w_0^2 n}{\lambda}, \tag{2.53}$$

z_R is Rayleigh range, and λ is the wavelength of the light, n is the index of refraction.

As mentioned, AC Stark shift, ΔE, is proportional to intensity, so optical potential can be written as

$$V_{\text{opt}} = -\Delta E_{\max} \left(\frac{w_0}{w(z)} \right)^2 \exp\left(\frac{-2s^2}{w(z)^2} \right), \tag{2.54}$$

where $\Delta E_{\max}$ is the maximum absolute AC Stark shift in the space, located at $(s = 0, z = 0)$, which is also regarded as optical trap depth. The negative sign indicates it is a trapping potential. Define z direction as axial direction, and any direction in xy plane as transverse direction. We will show along axial direction, the optical potential is a Lorentzian, and along transverse direction, it is a Gaussian.

Along transverse direction, we have

$$V_{\text{opt}}(z = 0, s) = -\Delta E_{\max} \exp\left(\frac{-2s^2}{w_0^2} \right) \tag{2.55}$$

$$= \Delta E_{\max} \left(-1 + \frac{2s^2}{w_0^2} - \dots \right) \tag{2.56}$$

$$\approx -\Delta E_{\max} + \frac{1}{2} m \omega_{\text{trans}}^2 s^2, \tag{2.57}$$

where m is mass of the trapped ion. In the second line, we take the Taylor expansion of the potential, and in the third line, we approximate the potential as a harmonic potential, hence we have

$$\omega_{\text{trans}} = \sqrt{\frac{4\Delta E_{\max}}{m w_0^2}} = \frac{2}{w_0} \sqrt{\frac{\Delta E_{\max}}{m}}. \tag{2.58}$$

Along the axial direction, we have

$$V_{\text{opt}}(s = 0, z) = -\Delta E_{\max} \left(\frac{w_0}{w(z)} \right)^2 \tag{2.59}$$

$$= -\Delta E_{\max} \left(\frac{1}{1 + (z/z_R)^2} \right) \tag{2.60}$$

$$= \Delta E_{\max} \left(-1 + \frac{z^2}{z_R^2} - \dots \right) \tag{2.61}$$

$$= \Delta E_{\max} \left(-1 + \frac{z^2 \lambda^2}{\pi^2 w_0^4 n^2} - \dots \right) \tag{2.62}$$

$$\approx -\Delta E_{\max} + \frac{1}{2} m \omega_{\text{axial}}^2 z^2, \tag{2.63}$$

hence we have

$$\omega_{\text{axial}} = \sqrt{\frac{2\lambda^2 \Delta E_{\max}}{\pi^2 m w_0^4 n^2}} = \frac{\lambda}{\pi w_0^2 n}\sqrt{\frac{2\Delta E_{\max}}{m}}. \tag{2.64}$$

Eq. (2.58) and (2.64) are showing the trap frequencies along transverse and axial direction, and we have

$$\omega_{\text{axial}} = \frac{\lambda}{\sqrt{2}\pi w_0 n}\omega_{\text{trans}} \tag{2.65}$$

If we take wavelength $\lambda = 500$ nm, beam waist $w_0 = 1$ μm, and index of refraction $n = 1$, we have $\omega_{\text{axial}} \approx 0.1\omega_{\text{trans}}$, axial trap frequency is much smaller than transverse trap frequency. Therefore, in this case, the Gaussian beam is only providing enough trapping for transverse direction. To compensate the weak trapping along axial direction, DC electrodes are used to provide axial trap frequency, creating static electric field confinement such that the trap frequencies along all 3 spacial directions are in similar order of magnitude.

2.4 Optical Trapping Lifetime

Trap frequencies determine whether ions can be trapped or not, but it does not determine the trapping lifetime. Optical trapping lifetime is determined by optical trap depth, and heating rate of the trapped ion system, which is the rate of temperature increase of the system. Calculating optical trapping lifetime is calculating optical trapping probability. As for trapping with a single ion, optical trapping probability is simply the probability for the ion does not escape the trap. If optical trapping probability is exponentially decrease in time, or can be approximated as an exponential function with respect to time, optical trapping lifetime can be defined as the time for trapping probability to reach $1/e$.

Energy-cutoff model, described in [12], is a simple analytic model describing a single ion in a single-beam optical dipole trap, and predicts the trapping probability. This model treats the system as a 3D harmonic oscillator, with the same trap frequencies in all 3 directions. Then, the total trap potential is

$$V_{\text{trap}}(x, y, z) = \frac{1}{2} m \omega_{\text{trap}}^2 r^2,$$

where

$$r^2 \equiv x^2 + y^2 + z^2.$$

This is a trap potential with infinite depth, but any real trap should have finite depth. We assume the trap depth is the same in all 3 directions, so we cut a line at $V_{\text{trap}}(x, y, z) =$

V_{depth}, where V_{depth} is optical trapping depth. We assume the trapped ion is lost if it has kinetic energy higher than V_{depth}, such that trapping probability is sum of the probabilities of the ion being in each motional state with eigenenergy lower than V_{depth}, and the probability of the ion being in each state can be calculated from a canonical ensemble. In this case, we are using a infinitely deep trapping potential to calculate the energy eigenstates, but we assume the ion is lost if it has an energy above V_{depth}.

For 3D harmonic oscillator, we know the partition function, Z_3, and density of states, $D_3(E)$, are

$$Z_3 \approx (\beta\hbar\omega)^{-3},$$

where $\beta \equiv 1/(k_B T)$, and

$$D_3(E) \approx \frac{E^2}{2\,(\hbar\omega)^3}.$$

Now, we can write optial trapping probability, p_{opt}, as

$$\begin{aligned} p_{\text{opt}} &= \int_0^{V_{\text{depth}}} \frac{1}{Z_3} D(E) \exp(-\beta E)\; dE && (2.66)\\ &= \int_0^{V_{\text{depth}}} \frac{1}{2}\beta^3 E^2 \exp(-\beta E)\; dE && (2.67)\\ &= -\exp(-\beta E)\left(\frac{\beta^2 E^2}{2} + \beta E + 1\right)\Bigg|_0^{V_{\text{depth}}} && (2.68)\\ &= 1 - \left(\frac{\beta^2 V_{\text{depth}}^2}{2} + \beta V_{\text{depth}} + 1\right)\exp(-\beta V_{\text{depth}}). && (2.69) \end{aligned}$$

Now, trapping probability p_{opt} is a function of U_{depth} and β. By intro ducting a new variable heating rate, H, where

$$H \equiv \frac{\Delta T}{\Delta t}.$$

Since optical trapping lifetime for a single ion is limited to few second [7], which is much smaller than conventional trapping lifetime, we assumed the heating rate is a constant in during the trapping lifetime. If we also assume V_{depth} is a constant, we have

$$p_{\text{opt}}(t) = 1 - \left(\frac{\beta(t)^2 V_{\text{depth}}^2}{2} + \beta(t) V_{\text{depth}} + 1\right)\exp(-\beta(t) V_{\text{depth}}), \tag{2.70}$$

where $\beta(t) \equiv 1/[k_B T(t)]$, $T(t) = T_0 + Ht$, and T_0 is initial temperature of the system. Optical trapping probability $p_{\text{opt}}(t)$ is a function of time, and trapping lifetime can be extracted by calculating $p_{\text{opt}}(t)$.

2.5 Searching for Ion Species

For optical trapping of neutral atoms, alkali-metal atoms are commonly used. Since alkali atoms have only one valence electron with a closed inner shell, we can approximately treat its internal states as single particle states, thus, it is easy to manipulate the states using lasers with appropriate wavelengths. If the internal states of a atom can be treated as single particle states, this atom will have a strong $S \rightarrow P$ manifold transition, since the ground internal state must be $S_{1/2}$ state. Moreover, lasers with wavelengths corresponding to the $S \rightarrow P$ transitions of alkali atoms are easier to prepare experimentally. As for optical trap of ions, similarly, alkali-like ions are the most favored candidates.

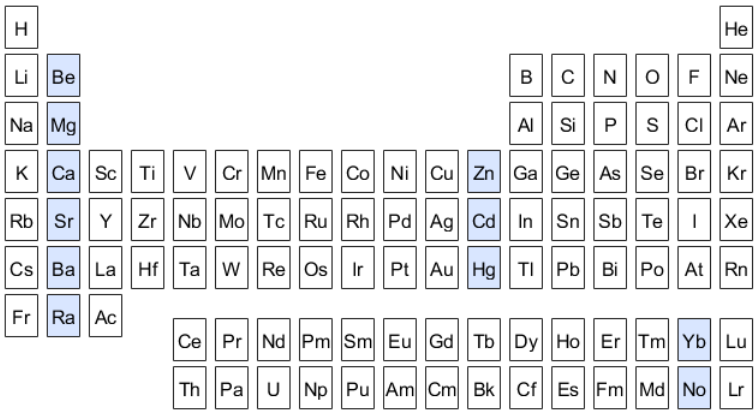

Figure 2.1: **Singly ionized alkali-like ions.**

Fig. 2.1 shows all alkali-like ions, if the atom is singly ionized, on periodic table. These ions have different $S \rightarrow P$ transition wavelengths and matrix elements, therefore they have different AC Stark shift and scattering rate.

Ion species	Frequency [THz]	Wavelength [nm]	A [s^{-1}]	μ [C·m]	$\Omega/\sqrt{I}$ [Hz · W $^{-1/2}$· m]
Ba^+	607.43	493.55	9.53 $\times 10^7$	2.016 $\times 10^{-29}$	5.25 $\times 10^6$
Ra^+	640.10	468.35	1.061 $\times 10^8$	1.966 $\times 10^{-29}$	5.12 $\times 10^6$
Sr^+	710.96	421.67	1.279 $\times 10^8$	1.844 $\times 10^{-29}$	4.80 $\times 10^6$
Ca^+	755.22	396.96	1.4 $\times 10^8$	1.763 $\times 10^{-29}$	4.59 $\times 10^6$
Yb^+	811.29	369.52	1.23 $\times 10^8$	1.484 $\times 10^{-29}$	3.86 $\times 10^6$
Be^+	957.20	313.20	1.1285 $\times 10^8$	1.109 $\times 10^{-29}$	2.89 $\times 10^6$
Mg^+	1069.3	280.35	2.57 $\times 10^8$	1.417 $\times 10^{-29}$	3.69 $\times 10^6$
Cd^+	1323.2	226.57	3.177 $\times 10^8$	1.145 $\times 10^{-29}$	2.98 $\times 10^6$
Zn^+	1453.4	206.27	3.86 $\times 10^8$	1.096 $\times 10^{-29}$	2.85 $\times 10^6$
Hg^+	1543.5	194.23	7.5 $\times 10^8$	1.396 $\times 10^{-29}$	3.63 $\times 10^6$

Table 2.1: **Transitions from $S_{1/2}$ to $P_{1/2}$ state of alkali-like ions.**

To judge which ion is a better candidate for optical trapping, we list the parameters that are relevant to AC Stark shift and scattering rate calculation in Table 2.1. In this table, ion species are ordered by their transition frequencies from $S_{1/2}$ to $P_{1/2}$ state, and Einstein A coefficient, A, transition matrix element, μ, and Rabi frequency per square root of laser intensity, $\Omega/\sqrt{I}$, are listed. Hyperfine levels of the ions are not considered, since we did not specify isotope number. In addition, No^+ is not listed in the table, since it has no stable isotope. Table 2.1 shows that Ba^+ ion has the smallest transition frequency and largest Rabi frequency at a given laser intensity, which means Ba^+ experience more AC Stark shift magnitude compared to other ions at the same laser detuning and intensity. This makes Ba^+ to be a potential candidate, however, AC Stark shift is not the only criterion to judge an ion.

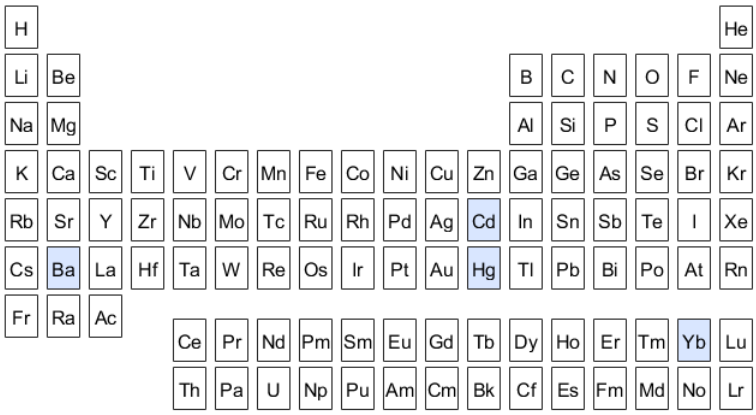

Figure 2.2: **Singly ionized alkali-like ions having isotope(s) with nucleus spin $I = 1/2$.**

We also want the ion to have a isotope with nuclear spin $I = 1/2$, since it will make state detection of the ion to be convenient. Fig. 2.2 shows there are only 4 alkali-like ions satisfy the condition, Ba^+, Yb^+, Cd^+, and Hg^+. Since AC Stark shift is proportional to Ω^2, from Table 2.1, we know Cd^+ and Hg^+ have much smaller AC Stark shift compared to Ba^+ and Yb^+, and since Cd^+ and Hg^+ are toxic, we will focus our discussion mainly on Ba^+ and Yb^+ ions.

For QIP experiments with trapped ion system, both Ba^+ and Yb^+ are commonly used ions with their own advantages and disadvantages. We will explore their properties by placing them under a 1064 nm laser, which is a typical high power laser. This laser is red detuned to $S_{1/2} \rightarrow P_{1/2}$ transition for both Ba^+ and Yb^+ ions, meaning its frequency is smaller than the transition frequency, and creates a negative AC Stark shift. Here, we will only discuss the magnitude of AC Stark shift. Since Ba^+ has a smaller transition frequency, which leads to a smaller laser detuning, and it also has a larger Ω, both of two conditions give Ba^+ a stronger AC Stark shift compared to Yb^+. However, the small detuning of Ba^+ leads to the problem of high scattering rate.

Since AC Stark shift scales as I/δ, while scattering rate scales as I/δ^2, using large laser detuning to minimize scattering rate is a much more efficient compared to lowering laser intensity. As for Yb^+, since it has a larger transition frequency, its high detuning under 1064 nm laser will strongly suppress the scattering rate. In particular, since 1064 nm laser has a high power, the high intensity can potential boost AC Stark shift to a desired magnitude.

Scattering rate to meta-stable D manifold is also an important criterion to an ion. Since AC Stark shift is a internal state dependent energy shift, when the ion scatter to D manifold, the trapping potential can become much shallower, or it can turn from a trapping potential to an anti-trapping potential. For Ba^+, the branching ratio for $P_{1/2} \rightarrow S_{1/2}$ versus $P_{1/2} \rightarrow D_{3/2}$ is about 3:1, whereas for Yb^+, this branching ratio is about 200:1. The probability for Ba^+ in $P_{1/2}$ state to scatter to $D_{3/2}$ is 25%, and for Yb^+ is 0.5%. This high scattering rate to meta-stable D state for Ba^+ strongly limits its optical trapping lifetime, as we will discuss this topic in Section 4.2.3.

Chapter 3

Optical Cavity Trap for 2D Ion Crystals

Up to now, optical trapping for 2D ion crystals is still a field without experimental exploration, and even conventional 2D Paul ion trap has not been experimentally achieved until recent studies [6, 13]. For optical trapping, as discussed in Section 1.1, the feasibility of trapping ions in a 1D linear chain is experimentally demonstrated [9]. The difficulty of extending the system to 2D comes from the shallow optical trap depth, since in practice, lasers have finite power, and they cannot be focus to arbitrary small waist. As we have shown in previous chapter, a small optical trap depth will lead to a short optical trapping lifetime, and also a small trap frequency. If the trap frequency is not high enough, the trapped ions will not transition to 2D structure. If the optical trap depth is not high enough, the system will not have long enough trapping lifetime to do any QIP experiment.

In this chapter, we will theoretically explore the feasibility of 2D optical ion trapping with a Gaussian beam plus an optical cavity. Intensity of the beam will get amplified by the cavity, creating a much higher AC Stark shift, which can potentially provide high enough optical trap depth. Moreover, the intensity distribution inside an optical cavity has a standing wave profile, such that ion can be trapped in the plane perpendicular to the direction of beam propagation, with a much higher trap frequency, which is now related to the wavelength of the beam.

First, we introduce what is an optical cavity. Then, we introduce our proposed optical cavity ion trap, by explaining its setup, trapping parameters, and two different trapping strategies. Finally, we investigate what are the required trapping parameters to trap ion crystals in 2D, by studying the properties of 2D ion crystals.

3.1 Optical Cavity

The simplest optical cavity consists of two parallel thin mirrors, separated by some distance d, which is called Fabry–Perot interferometer. We will exam how laser intensity get amplified by this Fabry–Perot interferometer by deriving a relation between electric field amplitude of incident electromagnetic wave and the electromagnetic wave inside the cavity, which is in between the two mirrors. Then, we will find out how to have standing wave intensity distribution inside the cavity.

To find the relation between electric field amplitude of incident and cavity electromagnetic waves, we will consider the electromagnetic waves as plane waves, travelling at the direction perpendicular to the mirrors, which we define it as z direction. In the real world, electromagnetic waves are never plane waves in large spatial scale, thus, this is an assumption. We have incident electromagnetic wave as

$$E_{\mathrm{I}}(z,t) = E_{0,\mathrm{I}} e^{i\omega t - kz}, \tag{3.1}$$

and cavity electromagnetic wave as

$$E_{\mathrm{cavity}}(z,t) = E_{0,\mathrm{cavity}}(t) e^{i\omega t - kz}, \tag{3.2}$$

where ω and k are angular frequency and wave vector of the electromagnetic wave, respectively. Consider the two mirrors are identical and separated by a distance of d, with electric field reflection and transmission coefficients r and t, which satisfy

$$r^2 + t^2 = 1. \tag{3.3}$$

The time for electromagnetic wave to circulate one round-trip is

$$\tau \equiv \frac{2d}{v} = \frac{2nd}{c}, \tag{3.4}$$

where $v = c/n$ is the speed of light in a medium with index of refraction n, which is filling the cavity, and time τ is called cavity round-trip time. Consider the incident wave enters the cavity at $t = 0$, then the wave inside the cavity at $t = \tau$ consist of two part. The first part is the wave transmitted through the mirror at $t = 0$. The second part is the wave transmitted through the mirror at $t = \tau$, and has propagate inside the cavity for a round-trip. We can write

$$E_{\mathrm{cavity}}(t=\tau) = E_{0,\mathrm{cavity}}(t) e^{i\omega\tau} = t E_{0,\mathrm{I}} e^{i\omega\tau} + r^2 E_{0,\mathrm{cavity}}(t) e^{i(\omega\tau - 2kd)}. \tag{3.5}$$

After many round-trip cavity times, e.g. at $t = m\tau$, the cavity will reach steady state, such that $E_{0,\text{cavity}}(t > m\tau)$ becomes a constant in time. Define $E_{0,\text{cavity}}(t = m\tau) \equiv E_{0,\text{cavity}}$, we can solve for

$$E_{0,\text{cavity}} = \frac{t}{1 - r^2 e^{-i\Delta}} E_{0,\text{I}}, \tag{3.6}$$

where

$$\Delta = 2kd$$

is the round-trip phase difference.

At cavity steady state, if the electromagnetic wave propagating at different directions satisfy

$$E_{\text{cavity}}(z,t) = E^{+}_{0,\text{cavity}} \cos(\omega t - kz) + E^{-}_{0,\text{cavity}} \cos(\omega t + kz) \tag{3.7}$$

$$= 2E_{0,\text{cavity}} \cos(\omega t) \cos(kz), \tag{3.8}$$

where $E^{+}_{0,\text{cavity}}$ and $E^{-}_{0,\text{cavity}}$ are electric field amplitude of two waves propagating at different directions, with $E^{+}_{0,\text{cavity}} = E^{-}_{0,\text{cavity}} = E_{0,\text{cavity}}$. Now, the electromagnetic wave inside the cavity is a standing wave, therefore, we need round-trip phase difference Δ equals to integer times 2π, which is

$$e^{-i\Delta} = 1.$$

Overall, we find that a standing wave cavity can amplify intensity of incident laser by

$$\frac{I_{\text{cavity}}}{I_{\text{I}}} = \frac{n_{\text{cavity}} |E_{0,\text{cavity}}|^2}{n_{\text{I}} |E_{0,\text{I}}|^2} = \frac{n_{\text{cavity}}}{n_{\text{I}}} \left(\frac{t}{1 - r^2} \right)^2, \tag{3.9}$$

where n_{cavity} and n_{I} are index of refraction for the mediums inside and outside the cavity, respectively.

Similarly, we can find the transmittance T of whole Fabry–Perot interferometer system is

$$T \equiv \frac{I_{\text{T}}}{I_{\text{I}}} = \frac{1}{1 + [4r^2/(1 - r^2)^2] \sin^2(\Delta/2)}, \tag{3.10}$$

where I_{T} and I_{I} are transmitted and incident laser intensity. We define the factor inside the square bracket as coefficient of finesse, F

$$F \equiv \frac{4r^2}{(1 - r^2)^2}, \tag{3.11}$$

and define cavity finesse, $\mathcal{F}$ as

$$\mathcal{F} \equiv \frac{\pi\sqrt{F}}{2} = \frac{\pi r}{1 - r^2}. \tag{3.12}$$

Cavity finesse $\mathcal{F}$ is an important parameter to characterize a cavity. From now on, we will use finesse to indicate how good a cavity is at amplifying laser intensity, e.g. by solving Eq. (3.9) and (3.12), taking all index of refraction as 1, we find a cavity with $\mathcal{F} = 3000$ has $r = 0.999477$, and $I_{\text{cavity}}/I_{\text{I}} = 955 \approx 1000$, which means a $\mathcal{F} = 3000$ cavity can amplify intensity by ~ 1000 times.

3.2 Optical Cavity Ion Trap

In this section, we propose a scheme to trap 2D ion crystals with optical cavity trap. As discussed in Section 2.3, optical trap depth is normally smaller conventional trap depth for ions by 5-6 orders of magnitude. This small trap depth limits optical trapping lifetime, and also brings difficulties of loading ions into the optical trap. Therefore, we load the ions into a conventional Paul trap, and have them trapped in 2D structure initially. Trapping 2D planar ion crystals in a linear Paul trap have been accomplished in a recent experiment [6]. Then, we apply laser cooling to the ions to bring its temperature below the optical trap depth, and adiabatically transfer the system to optical trapping, by ramping down the conventional trap strength while ramping up the optical beam intensity with certain rate. This adiabatic process must be slow enough such that the internal states of ions are unchanged, and also be fast compared to the optical trapping lifetime such that the remaining optical trapping period is still long enough to perform QIP experiments. A method of finding the best adiabatic transfer scheme is developed and discussed in Appendix. After the optical trapping period, we want to transfer the 2D ion crystal become to conventional trap to perform state detection. Since the detection is a measurement that causes the quantum state to collapse into the measured state, and AC Stark shift is a state dependent energy shift, performing state detection during optical trapping period can change the effective optical potential, which heat up the system, potentially causing the ions to escape the trap.

In this section, we explain the optical cavity setup, and find the relations between optical trapping parameters, i.e. trap depth and trap frequency, and optical cavity parameters, i.e. cavity finesse and laser parameters. Then we discuss two trapping strategies associated with trapping with red or blue detuned laser.

3.2.1 Trap Setup

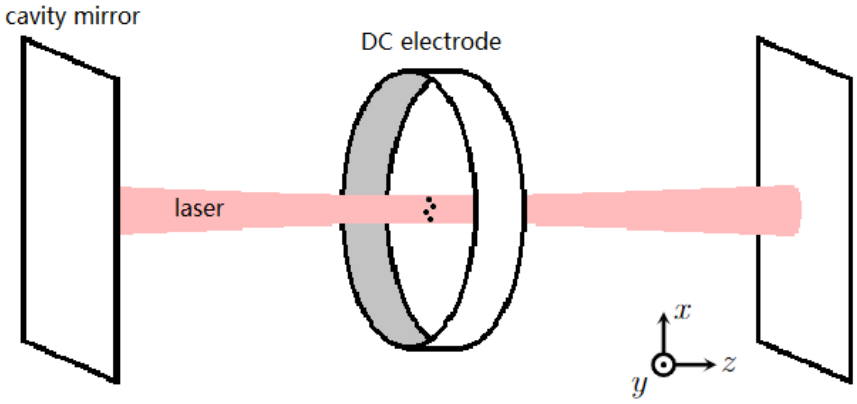

Figure 3.1: **Optical cavity trap setup.**

Optical cavity ion trap consists of a circular electrode and a optical cavity, aligned to the same axis along axial direction, as shown in Fig. 3.1. The circular electrode is applied with DC voltage, creating a static electric potential to the 2D ion crystal. This electric potential provides radial confinement in x and y directions. Meanwhile, a laser amplified by the optical cavity is providing axial confinement in z direction.

Since the size of trapped ion crystals are normally measured in unit of μm, the DC electrode is much larger than the trapped 2D ion crystal. Thus, electric potential offered by this DC electrode, denoted as V_{DC}, can be approximated as harmonic potential

$$V_{\mathrm{DC}}(x,y,z) = \frac{1}{2}m\left[\omega_{\mathrm{DC},x}^2 x^2 + \omega_{\mathrm{DC},y}^2 y^2 - \omega_{\mathrm{DC},z}^2 z^2\right], \tag{3.13}$$

with

$$\omega_{\mathrm{DC},z}^2 = \omega_{\mathrm{DC},x}^2 + \omega_{\mathrm{DC},y}^2, \tag{3.14}$$

where m is mass of the ion, $\omega_{\mathrm{DC},x}$ and $\omega_{\mathrm{DC},y}$ are trap frequencies of DC potential in x and y directions. This potential is created by static electric field, therefore we can verify that it satisfies Laplace's equation

$$\nabla^2\, V_{\mathrm{DC}} = 0.$$

Laplace's equation tells us, electric potential cannot provide trapping in all 3 spatial direction, hence, if we have trapping in x and y directions, the potential must be anti-trapping

in z direction. This anti-trapping DC potential in z will be compensated by optical potential created by laser intensity, to make a total trapping potential in all 3 direction. In addition, the shape of the electrode is not restricted to be circular, and it could be any shape such that it can provide a potential described by Eq. (3.13).

Optical potential is provided by a Gaussian laser beam, whose intensity is amplified by the optical cavity, and we consider the cavity has only lowest Gaussian cavity mode being excited, therefore cavity intensity also has a Gaussian profile. The optical potential inside the cavity trap is given by

$$V_{\text{opt}} = -V_{\text{opt,depth}} \left(\frac{w_0}{w(z)}\right)^2 \exp\left(\frac{-2(x^2+y^2)}{w(z)^2}\right) \cos^2\left(\frac{2\pi z}{\lambda_{\text{red}}}\right) \tag{3.15}$$

$$V_{\text{opt}} = V_{\text{opt,depth}} \left(\frac{w_0}{w(z)}\right)^2 \exp\left(\frac{-2(x^2+y^2)}{w(z)^2}\right) \sin^2\left(\frac{2\pi z}{\lambda_{\text{blue}}}\right), \tag{3.16}$$

where $V_{\text{opt,depth}}$ is optical trap depth, $w(z)$ is beam radius, $w_0 \equiv w(z=0)$ is beam waist, λ_{red} and λ_{blue} are wavelengths of red and blue detuned lasers. Optical trap depth V_{depth} is defined to be the maximum absolute value of AC Stark shift in space, which located maximum intensity point in space. Optical potential is expressed by two equations, since the optical potential created by red and blue detuned lasers are slightly different. Red detuned laser has frequency smaller than the atomic transition frequency, thus, laser detuning $\delta \equiv \omega_l - \omega_a < 0$, and the AC Stark shift of ground internal atomic state from red detuned lasers is negative. This means red detuned laser intensity lowers ground atomic state energy, hence, there is a minus sign in Eq. (3.15), and 2D ion crystal can be trapped in the plane of $z = 0$, where cavity intensity reaches maximum value. Blue detuned laser is an opposite case, whose laser detuning is positive, and its intensity rises ground atomic state energy, leading to a positive AC Stark shift. Hence, for blue detuned laser, 2D ion crystal need to be trapped in a plane of intensity minimum, and the sine square standing wave in Eq. (3.16) makes $z = 0$ to be the plane.

Total trap potential of optical cavity ion trap is the sum of DC and optical potential,

$$V_{\text{tot,trap}} = V_{\text{DC}} + V_{\text{opt}}. \tag{3.17}$$

Total potential energy of the trapped ion system consisting N ions is the sum of total trap potential on each ion, labeled by index i, and total Coulomb potential

$$V_{\text{tot}} = \left(\sum_{i=1}^{N} V_{\text{DC},i} + V_{\text{opt},i}\right) + V_{\text{Coulomb}}, \tag{3.18}$$

where total Coulomb potential is given by,

$$V_{\text{Coulomb}} = \sum_{i<j}^{N} \frac{e^2}{4\pi\varepsilon_0 \left\|\mathbf{r}_i - \mathbf{r}_j\right\|}. \tag{3.19}$$

Here, e, $\mathbf{r}_i$, and ε_0 are respectively electron charge, the position vector of ith ion, and the permittivity of free space. In next section, we will derive the trap frequencies offered by this trap potential $V_{\text{tot,trap}}$ in all spatial directions.

3.2.2 Trapping Parameters

Consider optical potential created by red detuned laser along z direction, from Eq. (3.15), we can write it as

$$V_{\text{opt}}(x = y = 0, z) = -V_{\text{opt,depth}} \left(\frac{w_0}{w(z)}\right)^2 \cos^2\left(\frac{2\pi z}{\lambda_{\text{red}}}\right). \tag{3.20}$$

Use Taylor expansion to expand it at $z = 0$, and the coefficient in front of term with z^2 indicates at $x = y = 0$, optical trap frequency along z is

$$\omega_{\text{opt},z} = \frac{2\pi}{\lambda_{\text{red}}} \sqrt{\frac{2}{m} V_{\text{opt,depth}}}, \tag{3.21}$$

which is similar to the method used in Section 2.3. Now, considering both optical and DC potential, the total z direction trap frequency at point $x = y = z = 0$ is

$$\omega_z = \sqrt{\frac{2V_{\text{opt,depth}}}{m} \left(\frac{2\pi}{\lambda}\right)^2 - \omega_{\text{DC},z}^2}. \tag{3.22}$$

This result can be generalized to both red and blue detuned lasers. The total z direction trap frequency depends on DC trap frequency, laser wavelength, and optical trap depth, which optical trap depth further depends on cavity finesse and parameters of the laser. However, this z direction trap frequency does not depend on cavity length. Therefore we have some freedom to pick a cavity length that is relatively stable against cavity intensity noise, or a length which is easier to be integrated into the full ion trap system.

Using similar way, we can find the total radial direction trap frequency at point $x = y = z = 0$ is

$$\omega_r = \sqrt{\frac{4V_{\text{opt,depth}}}{m{w_0}^2} + \omega_{\text{DC},r}^2}, \tag{3.23}$$

where we assumed DC potential has radial symmetry $\omega_{\mathrm{DC},x}^2 = \omega_{\mathrm{DC},y}^2 \equiv \omega_{\mathrm{DC},r}^2$, and ω_r can be trap frequency along any direction in xy plane. Normally, the optical contribution to total radial trap frequency is small, such that $\omega_r \approx \omega_{\mathrm{DC},r}$, but in the cases where optical potential depth is large, or beam waist w_0 is small, optical contribution to total radial trap frequency can be significant.

For both radial and axial directions, Taylor expansion of the total optical cavity trap potential have no r^1 or z^1 term, and the terms with power higher than 2 have small coefficients in front of them, compared to terms with r^2 and z^2. Therefore the total potential can be approximated as harmonic at small neighbourhood of point $x = y = z = 0$, but when the size of 2D ion crystal is big, or the laser beam waist is small, the ions will experience a strong inharmonicity from the potential. We will use trap frequencies in all spatial directions, beam waist w_0, and radius of the 2D ion crystal $r_{\max}$ to characterize total potential of the system. The ratio of trap frequencies in axial and radial direction is another important parameter, since if this ratio is small, the trapped ions will not form 2D structure. We call this ratio as trap aspect ratio, and denote is as α, where

$$\alpha \equiv \frac{\omega_z}{\omega_r}. \tag{3.24}$$

In later sections, we will numerically find the relation connecting structural phase transition point, trap aspect ratio α, and $w_0/r_{\max}$.

Now we want to know what is the total trap depth. Similar to total trap frequency, total total trap depth $V_{\mathrm{opt,depth}}$ is determined by both optical and DC potential. At $z \approx 0$, the local trapping potential along z direction can be written as

$$V_{\mathrm{tot,trap}}(x = y = 0, z) = -V_{\mathrm{opt,depth}} \cos^2\left(\frac{2\pi z}{\lambda}\right) - \frac{1}{2} m \omega_{\mathrm{DC},z}^2 z^2, \tag{3.25}$$

where total trap depth is the largest local maximum value of $V_{\mathrm{tot,trap}}(x = y = 0, z) - V_{\mathrm{tot,trap}}(x = y = z = 0)$. The value of total trap depth can be numerically calculated by solving

$$V_{\mathrm{opt,depth}} \sin^2\left(2\frac{2\pi z}{\lambda}\right) - m\omega_{\mathrm{DC},z}^2 z^2 = 0, \tag{3.26}$$

and the smallest nonzero solution is the z value where the total trap depth is located. Combining Eq. (3.25) and (3.26), we can find the value of total trap depth. Its value is determined by 3 parameters, $V_{\mathrm{opt,depth}}$, λ, and $\omega_{\mathrm{DC},z}$. However, for the cases we are studying, we normally have the optical potential to be the dominating term, such that

$$V_{\mathrm{tot,trap}}(x = y = 0, z) \approx -V_{\mathrm{opt,depth}} \cos^2\left(\frac{2\pi z}{\lambda}\right), \tag{3.27}$$

and

$$V_{\text{tot,depth}} \approx V_{\text{opt,depth}}. \tag{3.28}$$

For writing convenience, we will use $V_{\text{depth}} \equiv V_{\text{tot,depth}} \approx V_{\text{opt,depth}}$ to denote total trap depth.

The trap depth we find is only the trap depth along z direction. Since the confinement of ions along radial x and y direction is provided by DC potential, which has trap depth of $\sim eV \approx 10^4\ \text{K} \cdot k_B$. This trap depth is many orders of magnitude larger than z direction trap depth provided by optical potential, which is normally measured in unit of $\text{mK} \cdot k_B$. Therefore, when we need to estimate the stability of the system by considering the trap depth, we are referring to the trap depth along z direction.

3.2.3 Trapping with Red or Blue Detuned Laser

Recall in Section 2.1.1, we defined laser detuning δ as

$$\delta \equiv \omega_l - \omega_a, \tag{3.29}$$

where ω_l is laser frequency, and ω_a is atomic transition frequency. As discussed in Section 3.2.1, red detuned lasers have $\delta < 0$, whereas blue detuned lasers have $\delta > 0$. In other words, whether a specific laser is red or blue detuned depends on what is the atomic transition it is referring to. In Table 2.1, we see the $S_{1/2}$ to $P_{1/2}$ state transtition wavelength for Ba^+ is 493.5 nm, and for Yb^+ is 369.5 nm. For instance, the typical high power 1064 nm laser is red detuned for both Ba^+ and Yb^+.

From Eq. (3.15) and (3.16), we know both red and blue detuned lasers can provide trapping potential for ions, but trapping ions with red or blue detuned laser are very different. In Chapter 2, we discuss AC Stark shift and scattering rate are determined by laser detuning, meanwhile from Eq. (3.22) we can see lasers with different wavelengths provide different total trap frequency. Therefore, the trapping parameters offered by red and blue detuned lasers are completely different. More importantly, for red detuned lasers, ions are trapped in the plane of intensity maximum, while for blue detuned lasers, ions are trapped in the plane of zero intensity. If intensity is zero, the ions will not suffer from scattering, which is creating errors to QIP experiments as well as heating up the system. However, we need to assume the trapped ion system is initialized at zero temperature such that ions stay exactly at zero intensity plane, but we can never do this practically. The higher temperature the ions have, the further they can deviate from the zero intensity plane, and resulting higher scattering rate and heating rate. We would expect a nonlinear

temperature increase in a optical ion trap with blue detuned laser. Furthermore, the trapping probability may not be able to approximated as exponential function.

These concerns do not arise from optical ion trapping with red detuned lasers, and it indicates the lifetime and heating rate analysis for trapping with red and blue detuned laser should be very different. In this thesis, we will focus on trapping with red detuned lasers, especially with the high power 1064 nm laser, but we will discuss the scalable potential of blue detuned laser trapping in later chapters and in outlook.

3.3 Structural Phase Transition of 2D ion crystals

We have demonstrated optical cavity trap can provide confinement to a 2D ion crystal using DC and optical potential. However, before designing an optical cavity trap with some specific parameters, we need to know what are the required trapping parameters to trap ion crystals in 2D. To address this question, we need to introduce structural phase transition of 2D ion crystals. If the trap potential at ion crystal can be treated as harmonic potential locally, we can use trap frequencies to quantify the trap strength in each direction, and use trap aspect ratio, α, to quantify how stronger or weaker axial trap frequency is compared to radial trap frequency. For small α, the ion crystal will form a 1D linear chain, and by increasing α, the ion crystal will transition form 1D linear chain to a 3D zig-zag or 3D a spheroidal structure, and for very high α, the 3D structure will transition to a 2D planar structure. We want to know what are the α values for these transitions to occur, particularly for transition between 3D and 2D structural, but before that, we first need to know whether critical phase transition point exist or not.

In this section, we will first show the existence of critical structural phase transition point between 2D to 3D phases of ion crystals in harmonic potential, and come up with a way to precisely define critical structural phase transition point. However, 2D ion crystal can have more than one stable equilibrium positions under a given trapping potential, and critical structural phase transition points for different different equilibrium positions are different. Then, we will show some examples of different equilibrium positions of 2D ion crystals in optical cavity trap. Finally, we will numerically find the structural phase transition points as a function of equilibrium positions and ion number, and discuss how does our result connect to the analytic prediction [ref] of structural phase transition points.

3.3.1 Critical Transition Point

For ion crystals, structural phases are 1D, 2D, and 3D structure, and structural phases transition points are evaluated by trap aspect ratio α, which are analogous to phases transition points of substances measured by pressure and temperature. Critical structural phase transition points of ion crystals can be illustrated by using analogy with critical phase transition points of substances, e.g. water and alloy. At atmospheric pressure, solid to liquid phase transition of water has critical point of 0 °C, whereas liquid to gas phase transition has critical point of 100 °C. As for alloy, most alloy do not have a well defined critical phase transition points between different phases, since they are made of two or more different metals. By heating up a piece of solid alloy, it will becomes softer and softer as temperature increases, and gain liquidity gradually. We don not know whether structural phase transitions of ion crystals behave like water or alloy, so in this section, we will numerically explore how do ion crystals in harmonic potential transition between 2D and 3D structural phases.

To study this problem, we will numerically calculate the equilibrium positions of $N = 13$ $^{171}Yb^{+}$ ions in harmonic potential. To find the equilibrium positions, we first give the ions a initial guess of 3D positions, such that each ion has a position of (x, y, z) where x, y, and z are randomly generated. Then, we apply an optimization algorithm to find the local minimum potential energy of the trapped ion system described by Eq. (3.18) with respect to positions N ions. Starting from the initial guess, this optimization algorithm iteratively changes the positions of N ions by a small amount, until local minimum potential point is reached. The algorithm treats the potential energy as a function on $3N$ variables, and the resulting N-ion positions from local minimum potential point is the equilibrium position of the N-ion system. The local minimum point obtained in this way is not guaranteed to be global minimum point. Therefore, if the potential energy has multiple local minimum points, this means the numerical solution of equilibrium position is not unique, and which equilibrium position the algorithms is getting depends on the initial guess. From our numerical investigation, 2D ion crystal with $N = 13$ ions is a special case whose equilibrium position is unique under harmonic potential.

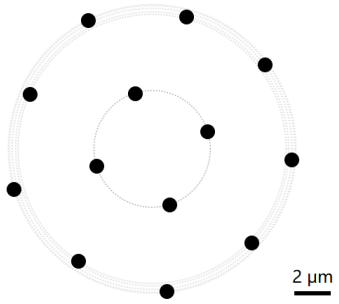

Figure 3.2: **Equilibrium position of 13 ions in 2D structural phase.** The result is numerically calculated by loading $N = 13$ $^{171}Yb^{+}$ ions into a harmonic potential with trap frequencies $\omega_r/2\pi = 0.5$ MHz and $\omega_z/2\pi = 1.5$ MHz.

The equilibrium position of $N = 13$ 2D ion crystal is presented in Fig. 3.2. The plot is calculated with trap aspect ratio $\alpha \equiv \omega_z/\omega_r = 3$, which is high enough for the system to transition of 2D structural phase. This calculated $N = 13$ ions configuration agrees with the detection image of experimentally trapped $N = 13$ 2D ion crystal in Paul trap [6].

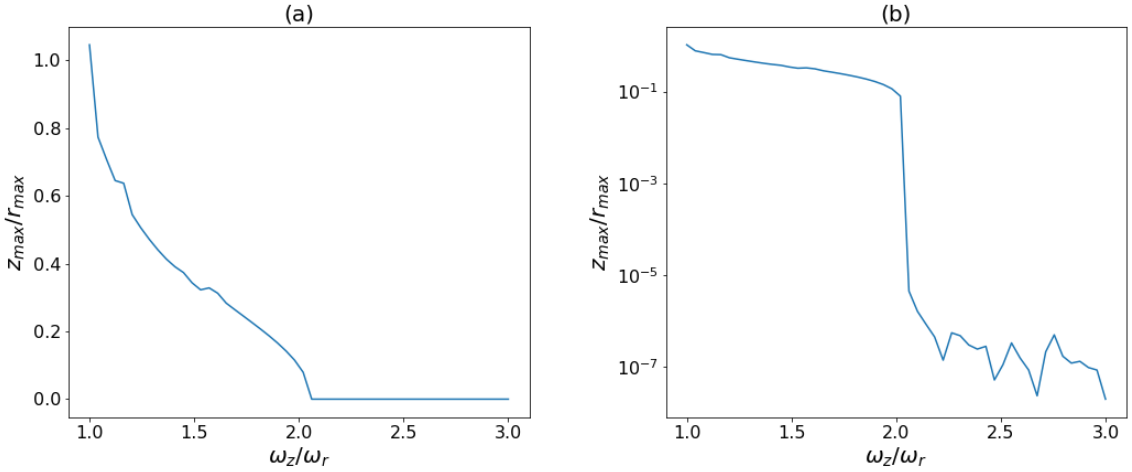

Figure 3.3: **Structural properties of trapped 13 ions in different trap aspect ratio.** This is numerically calculated with the same trapping parameters in Fig. 3.2, but with different $\alpha \equiv \omega_z/\omega_r$, by changing ω_z. For vertical axis, $z_{\max}$ and $r_{\max}$ are the maximum absolute value of z position and radial position of the trapped ions. The two plots are showing the same data with (a) vertical axis in linear scale and (b) vertical axis in log scale.

To see when the 2D to 3D structural transition occur, we numerically calculated the equilibrium positions with different α. In Fig. 3.3, structural properties of trapped 13 ions are characterized by $z_{\max}/r_{\max}$, where $z_{\max}$ is the maximum absolute value of z position of all ions, and $r_{\max}$ is the maximum radial position $r = \sqrt{x^2 + y^2}$. Since the center of trapped ion system is located at point $x = y = z = 0$, $z_{\max}$ and $r_{\max}$ are the maximum separation of ions from its center. For a 3D isotropic harmonic potential, we have $\alpha = 1$, and the figure is showing $z_{\max}/r_{\max} = 1$ as expected. In a particular small interval of α, near $\alpha = 2.1$, $z_{\max}/r_{\max}$ decreases exponentially as α increases, which can be clearly viewed in Fig. 3.3 (b), since a exponential decay in log scaled plot is presented as a linear line. This is a sign indicating critical structural phase transition point exists, and we now know which interval it is located.

To find the precise value of structural phase transition point, we can start by assuming the system is 2D and calculate its normal mode frequencies. As $\alpha \equiv \omega_z/\omega_r$ becomes smaller, z direction normal mode frequency of the trapped ion system becomes smaller. When the lowest z mode frequency reaches zero, keep decreasing α will cause the lowest z mode frequency to have no real solution, since our 2D assuming is not longer valid. Therefore, we can define structural phase transition point as the point where the lowest z direction normal mode frequency reaches zero, when assuming the ions equilibrium positions are always in 2D plane. This definition defines critical point by the transition from 2D to 3D, since we know critical point exists, it can be generalized to transition from 3D to 2D.

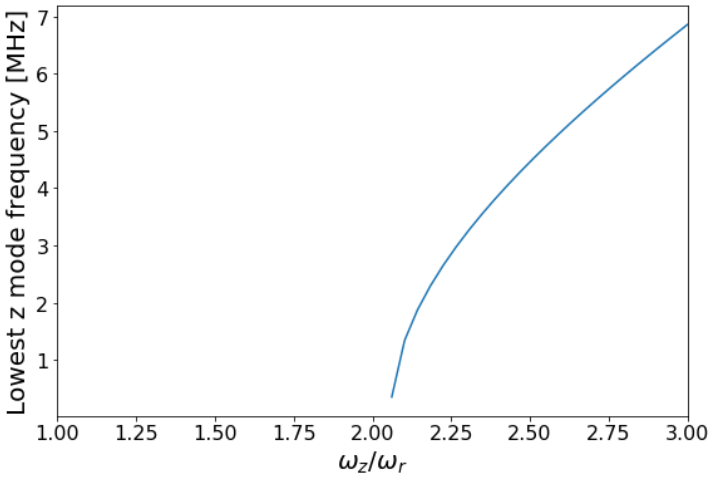

Figure 3.4: **Lowest z mode frequency of 2D ion crystal in different trap aspect ratio.** This is numerically calculated with the same trapping parameters in Fig. 3.3. The algorithm calculating ions equilibrium positions is assuming the space is 2D in xy plane.

To calculate normal mode frequencies, we need first obtain the equilibrium position. Since we assume the system is 2D, now we set the initial guess of ions' positions as 2D, therefore each ion is given with two random numbers as its initial (x, y) position. The optimization algorithm will also find the local minimum potential energy in a 2D space to get a 2D equilibrium position. The calculated results are shown in Fig. 3.4, and it tells us critical structural phase transition point for $N = 13$ ion between 2D and 3D phases is $\alpha = 2.1$.

3.3.2 Equilibrium Positions of 2D Ion Crystal

In last section, we saw an example of equilibrium position of 13 ions in harmonic potential. However, the equilibrium positions of 2D ion crystals in harmonic or optical cavity trap potential are not unique. This means it is possible to trap N ions in different 2D configurations under the same optical cavity trap potential. This is one of the intrinsic differences between 1D and 2D ion crystals, since the equilibrium position of 1D ion crystal in harmonic potential is unique.

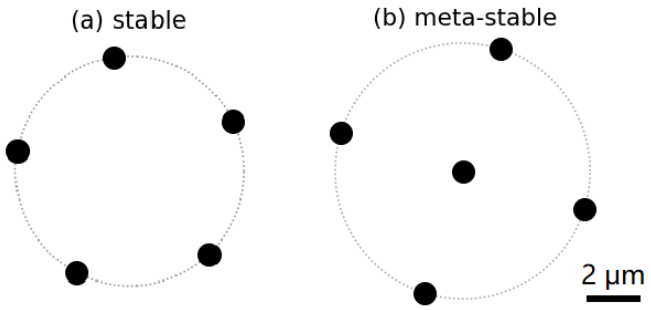

Figure 3.5: **Equilibrium positions of $N = 5$ 2D ion crystal.** The results are numerically calculated by loading $N = 5$ $^{171}Yb^{+}$ ions into an optical cavity potential with $\omega_r/2\pi = 0.5$ MHz and a sufficiently large axial trap frequency, and beam waist $w_0 = 100$ μm. The two equilibrium positions are (a) stable configuration with crystal radius $r_{\max} = 4.8$ μm, and (b) meta-stable configuration with $r_{\max} = 5.4$ μm.

2D ion crystal with $N = 5$ ions is the smallest ion number to have more than one equilibrium positions in optical cavity trap potential, as they are shown in Fig. 3.5. Stable equilibrium position is the configuration with the smallest potential energy among all other possible equilibrium positions, whereas meta-stable ones are the local minimum points of

potential energy. Stable and meta-stable configurations are labeled by their ion numbers in each ring, such as [5] and [1,4]. Different equilibrium positions also have different normal mode frequencies and eigenvectors.

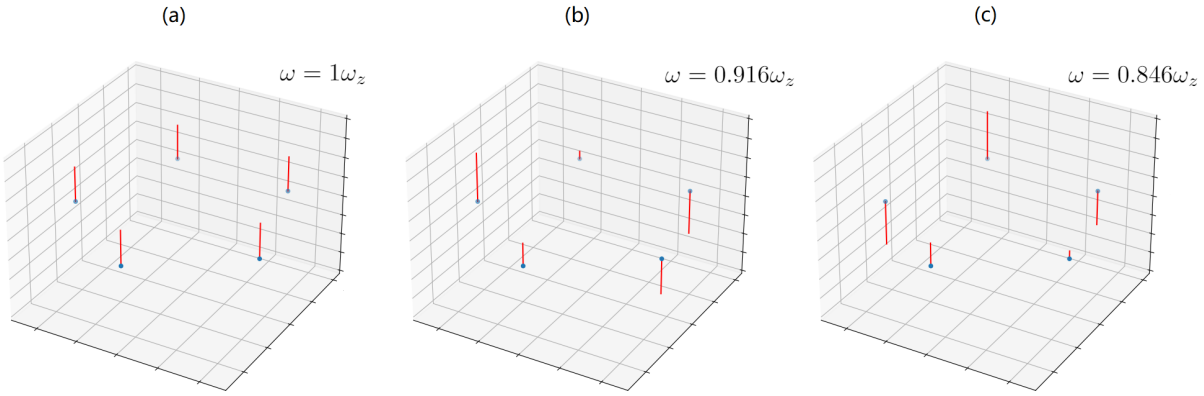

Figure 3.6: **Normal mode frequencies and eigenvectors in z direction for stable configuration of $N = 5$ 2D ion crystal.** This is numerically calculated with the same trapping parameters in Fig. 3.5. Both mode (b) and (c) have two-fold degeneracy due to radial rotational symmetry of the potential, thus there are 5 z modes in total.

The z direction normal mode frequencies and eigenvectors for $N = 5$ 2D ion crystals are shown in Fig. 3.6 and 3.7. Since the trapping potential has radial symmetry, the 2D ion crystals are free to rotate in xy plane without changing its potential energy, therefore some of the z modes are degenerate due to this symmetry. If a 2D ion crystal reach its 2D to 3D structural phase transition point, some ions will buckle first to turn into 3D structure, and this buckling of ions follows the directions of eigenvector of the lowest z mode.

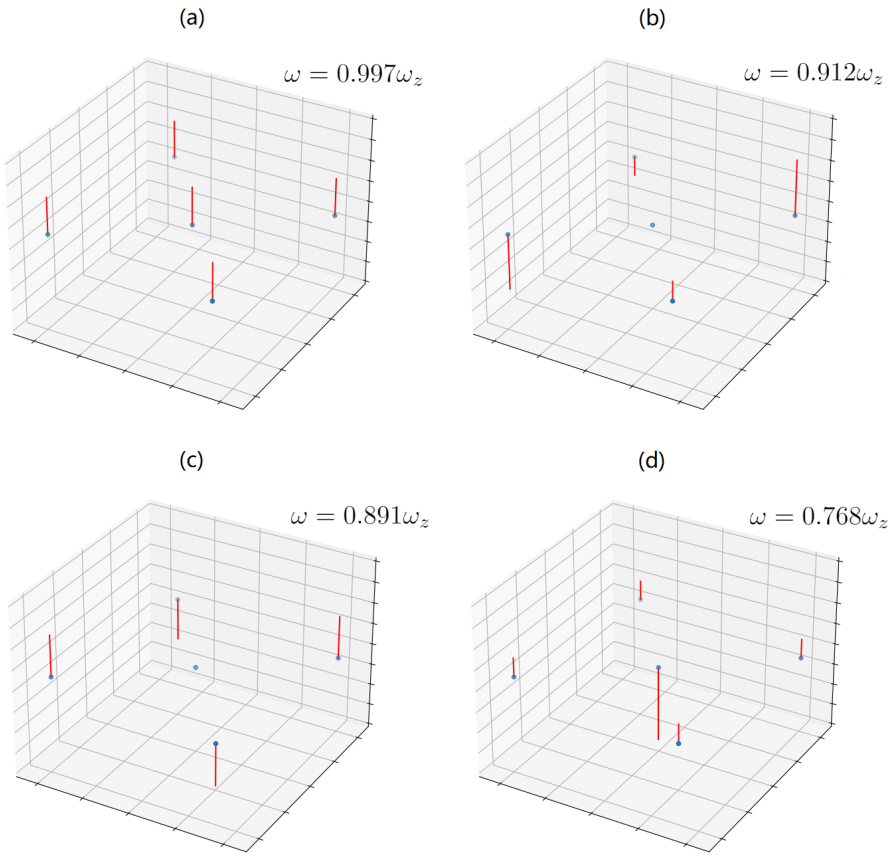

Figure 3.7: **Normal mode frequencies and eigenvectors in z direction for metastable configuration of $N = 5$ 2D ion crystal.** This is numerically calculated with the same trapping parameters in Fig. 3.5. The mode (b) has two-fold degeneracy due to radial rotational symmetry of the potential, thus there are 5 z modes in total.

We numerically calculated equilibrium positions of 2D ion crystals from $N = 5$ to $N = 30$, and present the results in Table 3.1. The equilibrium positions are generated by running the algorithms with different initial position guess, and the stable equilibrium position is the one with lowest potential energy among all other equilibrium positions. However, we do not claim the table lists all possible equilibrium positions, since randomly generated initial guess cannot guarantee to find all local minimum points of potential energy.

Ion number N	Stable equilibrium position	Meta-stable equilibrium position(s)
5	[5]	[1, 4]
6	[1, 5]	[6]
7	[1, 6]	
8	[1, 7]	
9	[2, 7]	[1, 8]
10	[2, 8]	[3, 7]
11	[3, 8]	
12	[3, 9]	[4,8]
13	[4, 9]	
14	[4, 10]	[5, 9]
15	[5, 10]	[1, 5, 9]
16	[1, 5, 10]	[5, 11]
17	[1, 6, 10]	[1, 5, 11]
18	[1, 6, 11]	[1, 7, 10]
19	[1, 6, 12]	[1, 7, 11]
20	[1, 7, 12]	[1, 7, 12(larger radius variance)]
21	[1, 7, 13]	[2, 7, 12]
22	[2, 8, 12]	[2, 7, 13]
23	[2, 8, 13]	[3, 8, 12]
24	[3, 8, 13]	[3, 9, 12]
25	[3, 9, 13]	[3, 8, 14]
26	[3, 9, 14]	[4, 9, 13]
27	[4, 9, 14]	[4, 10, 13]
28	[4, 10, 14]	[4, 9, 15]
29	[4, 10, 15]	[5, 10, 14], [4, 11, 14]
30	[5, 10, 15]	[4, 10, 16], [4, 11, 15], [1, 5, 10, 14]

Table 3.1: **Equilibrium positions of 2D ion crystals with $N = 5$ to 30 ions.** The results are numerically calculated by loading $^{171}Yb^{+}$ ions to an optical cavity potential with $\omega_r/2\pi = 0.5$ MHz and a sufficiently large axial trap frequency, and beam waist $w_0 = 100$ μm. Different equilibrium positions are obtained by feeding the algorithm with different initial position guess.

3.3.3 Structural Phase Transition Points

Since different equilibrium positions of 2D ion crystals have different normal mode spectrum and eigenvectors, we should expect structural phase transition points between 2D and 3D structures for different equilibrium positions are different, as we have defined transition points using the lowest z mode frequency in Section 3.3.1. In this section, we will explore structural phase transition points in optical cavity potential as a function of ions number N and its equilibrium positions, and the ratio of laser beam waist and ion crystal radius $w_0/r_{\max}$. First, we will take $w_0/r_{\max}$ to be large enough such that the radial inharmonic potential terms are negligible, and exam structural phase transition points at different ion numbers and equilibrium positions. Then, we fix N and equilibrium position, so that $r_{\max}$ is also fixed, to find how does structural phase transition points changes as a function of w_0.

The numerically calculated results for structural phase transition points and the fitting functions are shown in Fig. (3.8). The theoretically prediction of 2D to 3D structural phase transition points of ion crystals in harmonic trap are studied analytically and numerically in Ref. [14, 15]. In Ref. [14], the analytic perdition of transition points is that $\alpha \equiv \omega_z/\omega_r$ is proportional to $N^{0.25}$ with a good agreement to the numerically simulated results at large N, which is a simulation with up to $N = 500$ ions. In Ref. [15], $\alpha \propto N^{0.26}$ is obtained by fitting the numerically simulated results with $N = 10,\ 25,\ 70,\ 180,\ 500$. From the result shown in Fig. (3.8), we find for $N = 30$ to 120, $\alpha \propto N^{0.27}$ in optical cavity trap. The results in harmonic trap and optical cavity trap is close, but still different, since we did not introduce any errors for the trapping parameters. The only source of error is numerical error, which is negligible. This is what we should expect, since the trap potentials are similar, but slightly different. We think the difference comes from the different trapping potential used in the simulations, the different range of N, and the different transition points for different equilibrium positions. The transition points in optical cavity trap can teach us how choose the trapping parameters, and also provide guidance for scaling up the 2D trapped ion system.

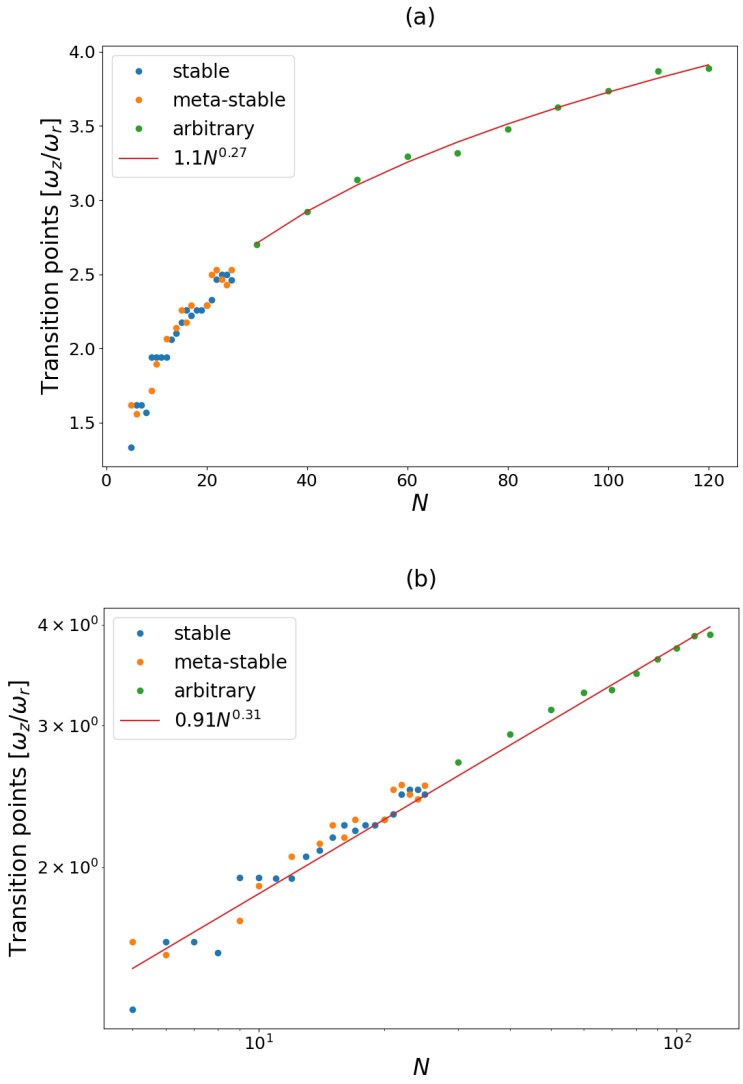

Figure 3.8: **Structural phase transition points for ion crystals in optical cavity trap.** The results are numerically calculated by loading N $^{171}Yb^{+}$ ions into an optical cavity potential with $\omega_r/2\pi = 0.5$ MHz and a sufficiently large axial trap frequency, and beam waist $w_0 = 100$ μm. The two plots have $x - y$ axes (a) in linear-linear scale and (b) in log-log scale. For small N, we show the transition points with stable and meta-stable equilibrium positions as blue and orange dots. For large N, we pick an arbitrary equilibrium position and show its transition points as green dots. The fitting function fits the data from stable and arbitrary equilibrium position.

As discussed in Section 3.2.2, optical cavity trap potential is not only characterized by trap frequencies, but also beam waist and 2D ion crystal radius. We now choose a fixed N to study how structural phase transition points changes respect to the ration of beam waist and 2D ion crystal radius. The result is showing in Fig. 3.9. If beam waist is smaller than two times the 2D ion crystal radius, structural phase transition points tends to increase by a large amount, which we do not want it to happen. This teaches us beam waist need to at least two times larger than 2D ion crystal radius.

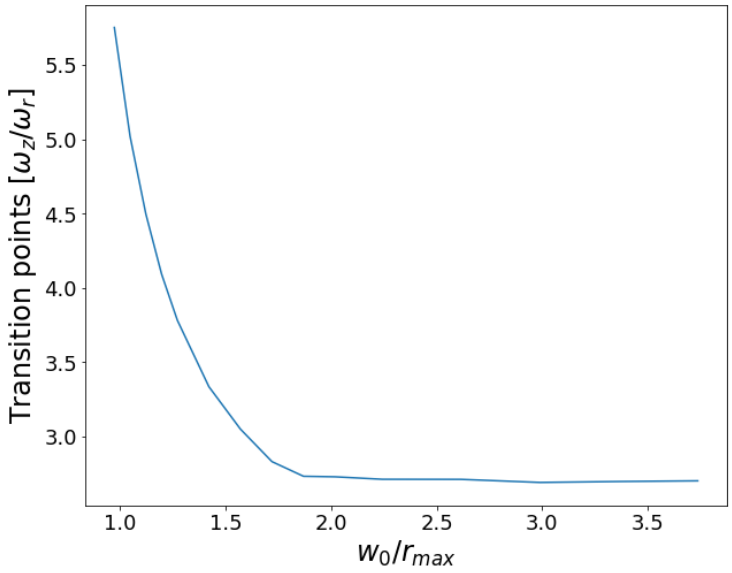

Figure 3.9: **Structural phase transition points for $N = 30$ ion crystals with different beam waist.** This is numerically calculated using stable equilibrium position of $N = 30$ 2D ion crystal of $^{171}Yb^+$ in an optical cavity potential with $\omega_r/2\pi = 0.5$ MHz and a sufficiently large axial trap frequency. The beam waist w_0 take values from 13-50 μm, and corresponding 2D ion crystal radius $r_{\max}$ is 13.37-13.38 μm.

3.4 2D Optical Cavity Ion Trap Design

In last section, we studied how the structural phase transition points change as a function trapping parameters. Now we can choose the trapping parameters based on the 2D ion trap we wish to build. In this section, we will provides several sets of trapping parameters for different N, by showing how those trapping parameters are related, i.e. if one need to change one or more parameters, how do other parameters change.

The first trapping parameter one need to choose is the DC trap frequencies, which determines the size of trapped 2D ion crystal. The choice of radial DC trap frequency specifies ion crystal radius, minimum ion spacing, and also provides an axial anti-trap frequency based on the value of radial trap frequency, as shown in Eq. (3.13). We want the minimum ion spacing to be large enough allowing individual addressing of ions with lasers, bu also want ion crystal radius to be small such that trapping beam waist is small, since in last section, we learned that beam waist must be at least two times the ion crystal radius. It is necessary to introduce a small asymmetry in radial DC trap frequencies, e.g. $\omega_y = 1.1\omega_x$, to prevent the 2D ion crystal to freely rotate in radial direction, which corresponds to the zero-frequency rotational mode.

After choosing DC trap frequencies and laser beam waist, if we assume the ion crystal will be trapped in 2D, the stable equilibrium position of each N is now well defined. To maintain the ion crystal in 2D phase, we need to provide enough axial trap frequency from optical potential, which is described by Eq. (3.22), and the undetermined parameters are optical trap depth V_{depth} and laser wavelength λ. In Section 3.2.3, we discussed the pros and cons of trapping ions with different laser wavelengths, and as mentioned, we will use $\lambda = 1064$ nm laser. Since the analysis of structural phase transition points tells us the minimum axial trap frequency to trap ion crystals in 2D, we can use it to calculate the minimum required optical trap depth. From the AC Stark shift calculation, optical trap depth can be converted to cavity laser intensity, which depends on incident laser intensity and cavity finesse via Eq. (3.9) and (3.12).

Overall, all trapping parameters are related except cavity length and mirrors' radii of curvature, which define the stability parameter g of a cavity

$$g_1 = 1 - \frac{L}{R_1} \tag{3.30}$$

$$g_2 = 1 - \frac{L}{R_2}, \tag{3.31}$$

where L is cavity length, R_1 and R_2 are the radii of curvature of two mirrors. A stable cavity must satisfy condition.

$$0 \leq g_1 g_1 \leq 1. \tag{3.32}$$

For 2D optical cavity trap, we propose utilizing near-concentric cavity, for which $R_1 = R_2 \approx L/2$, since it has a small and adjustable beam waist.

Ion number N	5	19	30
DC radial trap frequency	$2\pi \times 0.5$ MHz		
Laser wavelength	1064 nm		
Minimum ion spacing	5.7 μm	5.3 μm	4.4 μm
Ion crystal radius	4.8 μm	11 μm	13.4 μm
Laser beam waist	10 μm	22 μm	28 μm
Minimum AC Stark shift	230 MHz $\cdot$ h	430 MHz $\cdot$ h	565 MHz $\cdot$ h
Minimum cavity intensity	7.4×10^{11} W/m^2	1.4×10^{12} W/m^2	1.82×10^{12} W/m^2
Cavity finesse	3000		
Minimum laser power	120 mW	1.1 W	2.4 W
Scattering rate	2.3 s^{-1}	4.3 s^{-1}	5.6 s^{-1}

Table 3.2: **Trapping parameters for 2D optical cavity trap.** The ion is $^{171}Yb^+$. For each N, the parameters are determined for the stable equilibrium position of the ion crystal.

The required trapping parameters for 2D optical cavity trap are listed in Table 3.2, for 3 different choices of N. For 1064 nm laser, one can easily obtain ~ 10 W of power, therefore trapping up to 30 $^{171}Yb^+$ ions in 2D is feasible if we only looking at trapping parameters, i.e we did not consider trapping lifetime. We pick $N = 19$, since this is the maximum N that used in the 2D linear Paul ion trap [6], and we need to first load the ions into a Paul ion trap, then adiabatically transfer it to an optical cavity trap. The $N = 30$ case shows the ion crystal which can be trapped is scalable with respect to N, but in next chapter, we will find the difficulties for scalability of the system come from trapping lifetime. The parameters listed in Table 3.2 are not the recommended parameters, since the minimum cavity intensity is the smallest value such that the system can be constrained in 2D, and this value is determined by numerical calculation of structural phase transition point and AC Stark shift. The minimum laser power is determined by minimum cavity intensity, cavity finesse, and laser beam waist, since intensity is proportional to power, and inverse of beam waist square $1/w_0^2$.

To conclude, it is feasible to trap $N = 30$, and possibly more, $^{171}Yb^+$ ions in optical cavity trap in 2D, but at this stage, we do not know the stability and trapping lifetime of the system. We will study the stability and trapping lifetime in next chapter.

Chapter 4

Stability and Normal Mode Analysis of 2D Ion Crystal

In previous chapters, we show 2D ion crystal can be trapped in optical cavity trap with some experimentally realistic trapping parameters. However, we do not know the trapping lifetime of this system. If trapping lifetime is too short to do some interesting QIP experiments, 2D ion trapping with optical cavity is still not a feasible approach. More importantly, we do not know the stability between different equilibrium positions. If the potential barrier between two different equilibrium positions is smaller than the kinetic energy of the trapped ion system, the system will have a high probability of transitioning between the two equilibrium positions. Since different equilibrium positions have different normal mode frequencies and eigenvectors, it is difficult to perform QIP experiments to such an unstable system.

In this chapter, we will first numerically investigate potential barrier between different equilibrium positions. If the potential barrier is larger than trap depth, the equilibrium position will be stable in the sense of not transitioning to another equilibrium position during optical trapping period. Then, we will estimate optical trapping lifetime by estimating the heating rate of the system. Finally, we will numerically study how normal modes are affected by trapping parameters.

4.1 Potential Barrier between Equilibrium Positions

Different equilibrium positions of 2D ion crystals have different potential energy, but potential barrier between equilibrium positions are not the differences of their potential energy.

When a 2D ion crystal transitioning from one equilibrium position to another, the system must follow a continuous path in the configuration space with $2N$ dimensions, since there are N ions in total, and each ion has two x and y positions, meanwhile we are assuming the axial trap frequency is large enough to constrain the system in $z = 0$ plane. Therefore, each point on this path refers to a N-ion-position which has a total potential energy, and the highest total potential energy along the path is called potential peak. There are infinitely many continuous paths connecting two equilibrium positions, and each path has a potential peak. Potential barrier between two equilibrium positions is defined as the potential peak along the path with smallest potential peak among all continuous paths connecting the two two equilibrium positions. We choose this definition since the system will likely follow the path with smallest potential peak during transition, and if the system does not have kinetic energy higher than the potential barrier, it cannot reach the second equilibrium position.

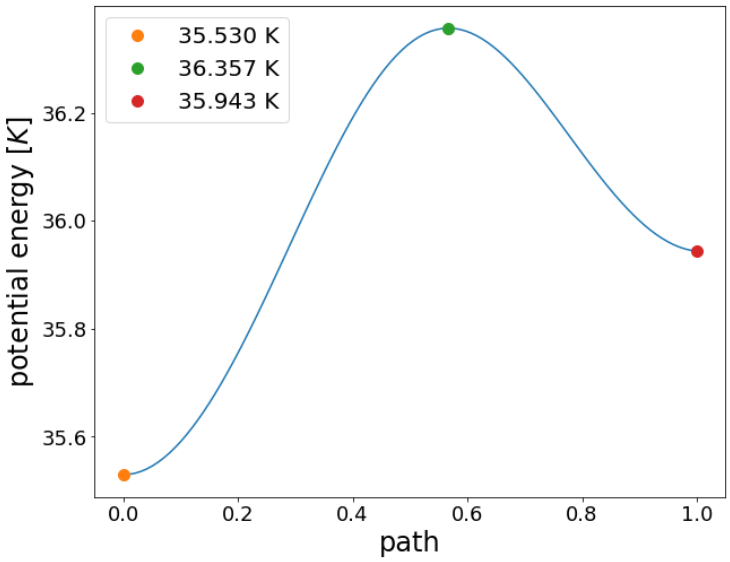

Figure 4.1: **Potential energy along the straight path between the two equilibrium positions of $N = 5$ 2D ion crystal.** This is numerically calculated by loading $N = 5$ $^{171}Yb^{+}$ ions into an optical cavity potential with radial trap frequency $\omega_r/2\pi = 0.5$ MHz and a sufficiently large axial trap frequency, and beam waist $w_0 = 50$ μm. Orange dot: potential energy of stable equilibrium position. Green dot: maximum potential energy along the straight path. Red dot: potential energy of meta-stable equilibrium position.

Before finding the correct path which gives us the potential barrier, let us first look

at how potential energy changes along the straight path where every ion in the initial equilibrium position moves straightly to its final position forming the final equilibrium position. To do this, every ion must know which is the final position it is going to such that total path length of the N ions is minimized. In other words, each ion in initial position must have a unique finial position. Therefore, we label all ions in initial equilibrium position and consider them as a set, while the ions in final equilibrium position as another set, and find out all possible bijections between the two sets. There are $N!$ bijections in total, and for each case, we numerically calculated the sum of ions' separations between initial and final position. The straight path is corresponds to the bijection with smallest total path length, which is the sum of ions' separations.

In Fig. 4.1, we use a variable called path to define the ratio of current path length and total path length for each ion. The potential energy difference between maximum point and stable equilibrium position is 827 mK, and the difference between maximum point and meta-stable equilibrium position is 413 mK. The value of potential energy depends on the choice of radial trap frequency, but we can compare this result to the result calculated from a numerically optimized path which gives us the potential barrier.

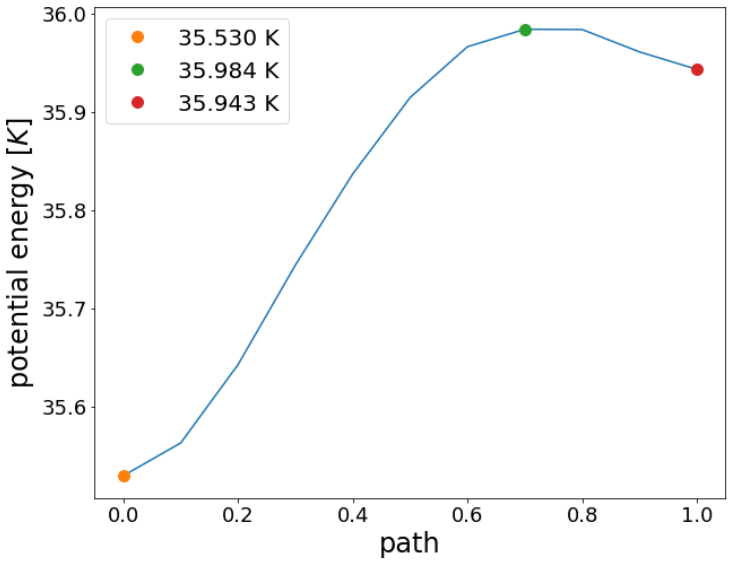

Figure 4.2: **Potential energy along the numerically optimized path between the two equilibrium positions of $N = 5$ 2D ion crystal.** This is numerically calculated with the same trapping parameters in Fig. 4.1. Orange dot: potential energy of stable equilibrium position. Green dot: maximum potential energy along the straight path. Red dot: potential energy of meta-stable equilibrium position.

In Fig 4.2, The potential energy difference between maximum point and stable equilibrium position is 454 mK, and the difference between maximum point and meta-stable equilibrium position is 41 mK. By comparing to the result in Fig. 4.1, the numerically optimized path lowered the potential peak by $\sim$ 370 mK. This indicates the meta-stable equilibrium position of $N = 5$ 2D ion crystal is much more unstable than the stable equilibrium position.

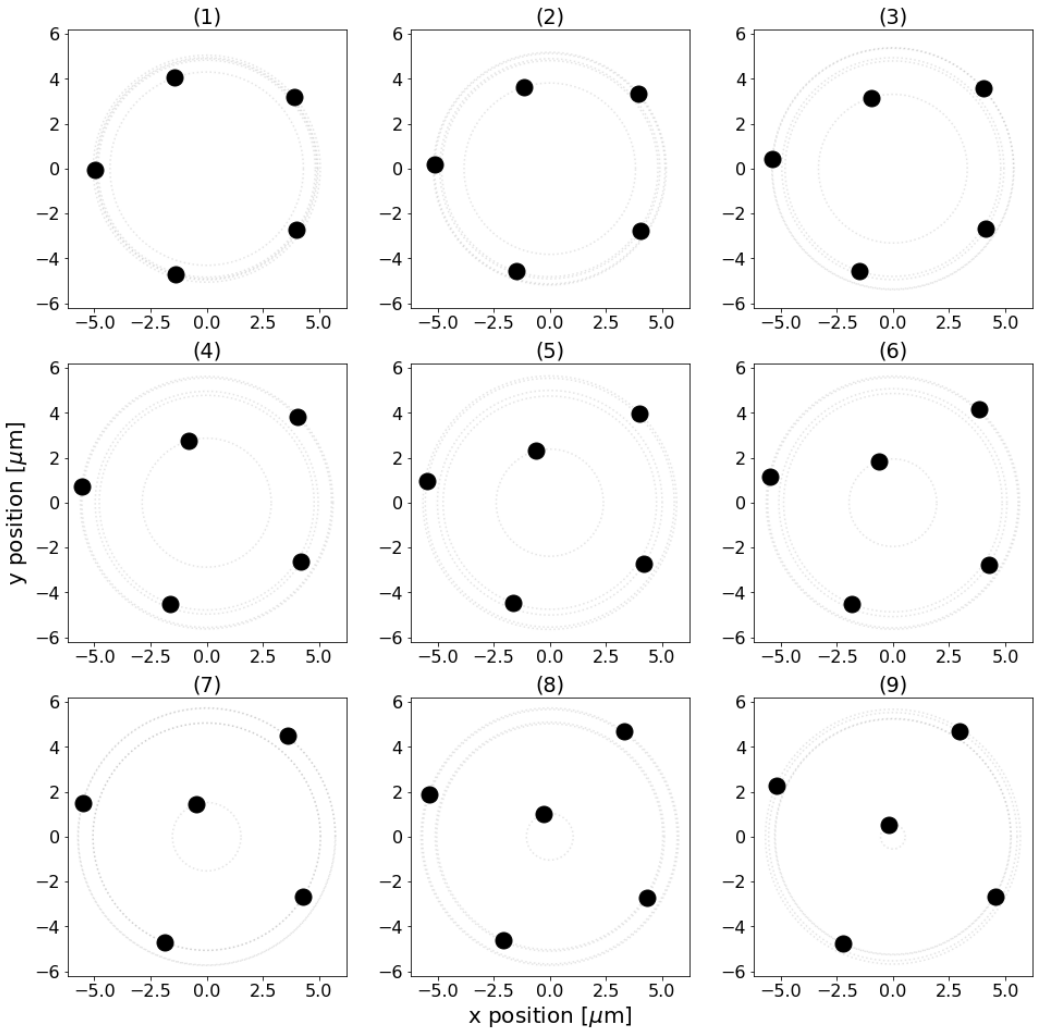

Figure 4.3: **Ions positions along the numerically optimized path between the two equilibrium positions of $N = 5$ 2D ion crystal.** The subplot (1) to (9) are 9 intermediate steps between the two equilibrium positions along the path in Fig.4.2.

The numerically optimized path is presented as 5-ion-position in the 9 subplots of Fig. 4.3. Subplot (1) starts from the stable equilibrium position, corresponding to the potential energy at path = 0 in Fig 4.2. Subplot (9) reaches to the meta-stable equilibrium position, corresponding to the potential energy at path = 0 in Fig 4.2. From Fig. 4.3, we can see only the center ion is roughly moving along a straight path, while others are not. The two neighbouring ions of the center ion is first pushed outwards as the center ion is moving, and then come backwards to its final positions.

Finding this correct path which gives us the potential barrier is not a easy problem. We need to numerically optimize the path in the $2N$ dimensional configuration space, therefore the computational power needed to obtain the correct path scales up exponentially with ion number N. Calculating the result in Fig 4.2 is much harder than the one in Fig. 4.1, especially for large N. This is the reason why the curve in Fig 4.2 is not as continuous as the one in Fig. 4.1.

To optimize the path in the $2N$ dimensional configuration space, we divide the path into n steps, where each step corresponds to a N-ion position, and note that this position does not need to be equilibrium position. Each N-ion position can also be regarded as a point in the $2N$ dimensional configuration space, and for each point, we apply the following algorithm to find the $(i+1)$th step from ith step:

1. In ith step, define a neighbourhood space of the point in the $2N$ dimensional configuration space, which is a set of N-ion positions that are close enough to the point. In addition, we judge closeness base on the path length of each ion, e.g. if there exists an ion which does not move much distance between the two equilibrium positions, its neighbourhood subspace will be small.

2. Select all points in the neighbourhood space that is closer to the final equilibrium position by a predetermined distance.

3. Calculate the potential energy of all selected points in the neighbourhood space.

4. Assign each selected point with a normalized transition probability, which is analogous to Boltzmann probability distribution

$$p_j = \text{normalize}\left[e^{-(E_j - E_i)/k_B T}\right], \tag{4.1}$$

where E_i is potential energy of the N-ion position in ith step, E_j is potential energy of the selected point, k_B is Boltzmann constant, and T is a predetermined parameter which has unit of temperature. The probability is normalized such that $\sum p_j = 1$.

5. Choose one of the selected point as $(i+1)$th step based on transition probability p_j.

Starting from the initial equilibrium position, applying this algorithm iteratively to each step will help us to find a path leading to the final equilibrium position, since the selected points are always closer to the final position. If $E_j - E_i$ is positive, the probability makes sure that the points with lower potential energy are more likely to be chosen in $(i+1)$th step, since the smaller $E_j - E_i > 0$ is, the larger the probability is. If $E_j - E_i$ is negative, this means we have already found the potential peak, since we have reached and passed the peak of potential energy, therefore how we choose the probability will not affect the value of potential peak. In this way, we are more likely to find a path with small potential peak, but the value is not necessarily the minimum value. The potential peaks we obtained are upper bounds of the desired potential barrier. We will need to calculate pn different paths with this approach and take the smallest potential peaks as final result, where pn denotes path number.

If we calculate enough number of paths, we can obtain a potential peak close enough to the potential barrier. However, even the calculation for a single path is extremely difficult to perform on an ordinary computer, since the number of the points we need to consider in the neighbourhood space is too large. Suppose for each ion, we only consider 4 points in its neighbourhood subspace, where the 4 points can locate at its up, down, left, and right in the 2D space. In this case, for the neighbourhood space, we need to consider 4^{2N} points in total. If $N = 5$, we have $4^{2N} = 1048576 \approx 10^6$, which is around one million points. For each of these points, we need to calculate its distance between the final position, and we need to do this in each step, and each path. Calculating the distances cannot be avoided by transforming the N-ion positions between different coordinate systems. We use an approximation method to generate the date in Fig 4.2, where instead of defining large amount of points, we randomly sample $ns = 1000$ points in the neighbourhood space, and ns denotes number of points in the space.

To summarize the algorithm parameters, we have $n = 11$, $pn = 10$, $ns = 1000$, and $T = 1$ mK, where n is the number of steps in each path, pn is the number of paths, ns is the number of random points sampled in the neighbourhood space, and T is a parameter to determine the transition probability. We do not know if this is the optimized set of algorithm parameters such that the algorithm can generate the smallest potential peak with limited computational resources, but this set of parameters is good enough to produce a path with a much smaller potential peak than the one along straight path.

To conclude, since 41 mK is an upper bound of the potential barrier for meta-stable equilibrium position of $N = 5$ 2D ion crystal, if the potential depth is smaller than this value, the ion crystal can transit into another equilibrium position during optical trapping

period. The stable equilibrium position of $N = 5$ 2D ion crystal is much more stable compare to the meta-stable one. Since conventional trapping has a much higher trap depth compared to optical trapping, we can always temporarily turn off the cooling of ions in conventional traps to exam whether a particular equilibrium position of the 2D ion crystal stable enough against other equilibrium position(s). This examination can be done before transferring the system into optical trapping period. It is possible to calculate the potential barrier(s) of 2D ion crystals with large N, but the calculations need to be performed on more capable computing devices than personal computers.

4.2 Trapping Lifetime and Heating Rate Estimation

In Section 2.4, we introduce an analytic model calculating optical trapping lifetime for a single ion. This model can be extended to systems with multiple ions, if we know the motional density of states, and multi-ion heating rate. Motional density of states for multi-ion system can be calculated numerically, but we do not know how to convert single ion heating rate to multi-ion heating rate. Due to the presence of ions' interaction, the increase of energy for one ion will affect other ions. In addition, this model assumes trap depth along all directions are the same, however this does not apply to the optical cavity potential we are studying. It is hard to come up with a theoretical model predicting optical trapping probability of the optical cavity trap. In this section, we will not use any theoretical model, instead, we will do an order of magnitude estimation for trapping lifetime, based on the value of optical trap depth and total heating rate. Once the system has an energy higher or comparable to the trap depth, it is very likely to have some of its ions to escape the trap.

Optical trapping lifetime is defined as the time for trapping probability to reach $1/e$, where for single ion, trapping probability is the probability for the ion does not escape the trap. However, for multiple ions, trapping probability can lead to ambiguity, as it can be phrased as trapping population, or the probability for any ion does not escape the trap. We will define trapping probability as the probability for any ion does not escape the trap. If one or more ions leave the trap, the remaining ions will reach to a new equilibrium position, and the quantum state of the system will be altered due to the strong interaction between ions, which will destroy the quantum information of original system. Therefore, all ions must remain inside the trap after the QIP experiment.

The trap depth is normally around 1-100 mK$\cdot k_B$, e.g. 1 GHz AC Stark shift is 1 GHz$\cdot h$ = 48 mK$\cdot k_B$, the relations between AC Stark shift, laser power, and beam waist can be found in Table 3.2. The sources of heating rate includes:

1. Recoil heating from photon scattering.
2. Stray electric field fluctuation.
3. Collisions with background gas particles
4. The variation of effective optical potential in time,
   (a) which is caused by the changing internal states of ions, i.e. the scattering events of ions.
   (b) which is caused by cavity length fluctuation.
   (c) which is caused by cavity intensity fluctuation.

Recoil heating is caused by the photon scattering from ion. The scattered photon will be emitted to a random direction, and since photon carries momentum, the photon will provide a "momentum kick" to the ion at the opposite direction. This recoil heating can be easily calculated by

$$E_{\text{rec}} = \frac{p^2}{2m} = \frac{h^2}{2\lambda^2 m} = 6.83 \times 10^{-31}\ \text{J} = 4.95 \times 10^{-5}\ \text{mK} \cdot k_B, \tag{4.2}$$

where p is momentum, h is Planck constant, we substitute the mass of $^{171}\text{Yb}^+$, $m = 171$ u $= 2.84 \times 10^{-25}$ kg, and wavelength of $\lambda = 1064$ nm. This E_{rec} is the increase of energy for a single ion per scattering event. If we consider 100 ions with scattering rate of 10 s^{-1} for each ion, the resulting recoil heating rate is still smaller than trap depth by orders of magnitude. By the time we have the estimation of other sources of heating rate, we will have more quantitative reasons to say this recoil heating rate is negligibly small.

As for heating induced by stray electric field fluctuation, the main source of stray electric field is caused by the laser ionized nonconducting part of the trap device, or the electrode patch fields. We do not have a good theoretical way to estimate the strength of stray electric field, but since the cavity amplified laser field is much stronger than the laser without cavity, and laser with near infrared 1064 nm wavelength is hard to ionize materials, we think heating rate caused by electric field fluctuation is also small. Therefore, we will focus on the estimation and analysis of heating rate due to collision with background gas particles, and the variation of effective optical potential in time.

4.2.1 Background Gas Collision

In linear Paul traps, ions are trapped in a vacuum chamber, but it is not perfect vacuum. Since ions carry charges, it can polarize the particles in the environment and interact with them. The majority of background gas particles in vacuum chambers are H_2 molecules [16], since the chamber walls are made of molten steel which contain Hydrogen. This interaction is described by Langevin collision model, where by polarizing the H_2 gas molecules, the ion provide a potential of

$$V(r) = -\frac{1}{2}p(r)E(r) = -\frac{\alpha e^2}{8\pi\varepsilon_0 r^4}, \tag{4.3}$$

where e is electron charge, ε is the vacuum permittivity, α is polarizability of the gas molecule, $r = \sqrt{x^2 + y^2}$, $E(r) = e/(4\pi\varepsilon_0 r^2)$ is the electric field of the ion, $p(r) = 4\pi\varepsilon_0 \alpha E(r)$ is the induced electric dipole moment of the gas molecule. Note that in Eq. (4.3), polarizability α is in centimetre–gram–second (CGS) unit for electromagnetism, such that for H_2 molecules, we have $\alpha = 0.787$ Å^3. To convert α in CGS unit to SI unit, one can use

$$\alpha'(\mathrm{C}\cdot\mathrm{m}^2\cdot\mathrm{V}^{-1}) = 10^{-30}\cdot 4\pi\varepsilon_0\,\alpha(\text{Å}^3), \tag{4.4}$$

and the conversion factor $4\pi\varepsilon_0$ is included in Eq. (4.3) and all other equations including α. In addition, Eq. (4.3) is also assuming the ion is always located at $r = 0$.

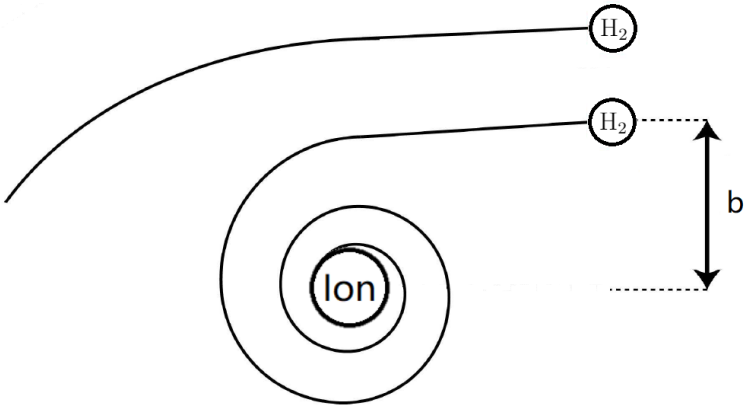

Figure 4.4: **Illustrative trajectories of gas particles in Langevin collision model.**

The word "collision" does not properly describe the interaction between the ion and gas molecules, since particles in Langevin collision model are not treated as hard spheres. The

illustrative trajectories of gas molecules are shown in Fig. 4.4, where the impact parameter b is defined as the separation between the ion and the gas molecule along the direction perpendicular to gas molecule's initial velocity in the plane of motion. For small b, the gas molecule will be captured by the ion and follow a spiral trajectory before it hit the ion, resulting a large energy exchange between the two particles. For large b, the interaction will deflect the gas molecule's trajectory, and only small amount of energy of the gas molecule is transferred to the ion. There exists a critical separation such that the ion will capture the gas molecule if b is small than its value, and we denote this critical separation as b_{crit}. This critical impact parameter is dependent on the speed of the gas molecule

$$b_{\text{crit}} = \left(\frac{\alpha e^2}{\pi\varepsilon_0\mu v_0^2}\right)^{1/4}, \tag{4.5}$$

where v_0 is initial speed of the gas molecule before interaction, μ is reduced mass of the ion and the gas molecule, which is defined as

$$\mu = \frac{m_{\text{Yb}} m_{\text{H}_2}}{m_{\text{Yb}} + m_{\text{H}_2}}, \tag{4.6}$$

where we are considering the two particles as Yb^+ ion and H_2 molecules. Langevin collision rate is the rate that gas molecules colliding with the ion with impact parameter $b < b_{\text{crit}}$, which is the number of gas molecules passing through an area of

$$\sigma_{\text{Lgvn}} = \pi b_{\text{crit}}^2 = \frac{\pi e}{v_0}\sqrt{\frac{\alpha}{\pi\varepsilon_0\mu}} = \frac{e}{v_0}\sqrt{\frac{\pi\alpha}{\varepsilon_0\mu}} \tag{4.7}$$

where σ_{Lgvn} is called Langevin collision cross section. Therefore Langevin collision rate is

$$r_{\text{Lgvn}} = n\sigma_{\text{Lgvn}} v_0 = ne\sqrt{\frac{\pi\alpha}{\varepsilon_0\mu}}. \tag{4.8}$$

At the end, We find that Langevin collision rate r_{Lgvn} is independent of speed v_0.

At room temperature, $T = 300$ K, the most probable speed of H_2 molecule is

$$v_{\text{p}} = \sqrt{\frac{2k_B T}{m_{\text{H}_2}}}, \tag{4.9}$$

thus at room temperature, H_2 molecules are most likely to have kinetic energy of

$$\frac{1}{2} m_{\text{H}_2} v_{\text{p}}^2 = k_B T = 300\ \text{K} \cdot k_B. \tag{4.10}$$

Since the optical cavity trap has trap depth $\sim 100\ \mathrm{mK} \cdot k_B$, a small fraction of energy from one H_2 molecule might be enough to knock the ion out of the trap, therefore we are interested to numerically calculate the collision with $b > b_{\mathrm{crit}}$.

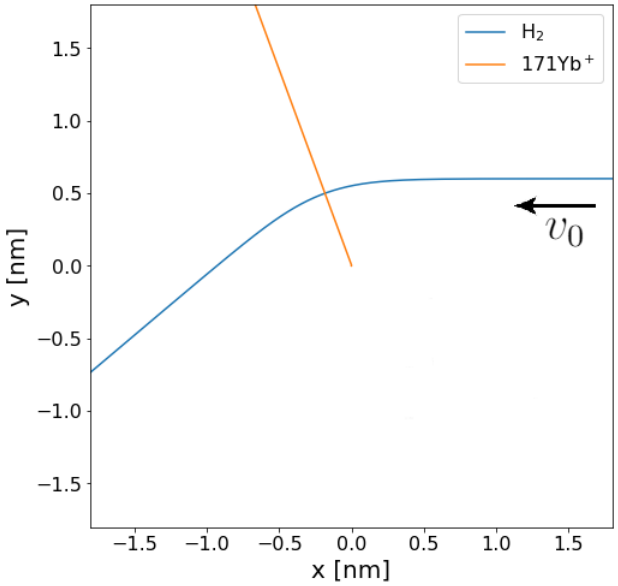

Figure 4.5: **Numerically calculated Yb^+ and H_2 collision trajectories.** The Yb^+ ion and H_2 have masses of 171 u and 2 u respectively, and the H_2 molecule has polarizability of $\alpha = 0.787\ \text{Å}^3$, impact parameter $b = 1.1\, b_{\mathrm{crit}}$, and initial speed $v_0 = 1579$ m/s, which is the most probable speed at $T = 300$ K. The Yb^+ ion is initially at rest and gain a kinetic energy of $1.65\ \mathrm{K} \cdot k_B$ at the end.

To simulate the dynamics of one Yb^+ ion and H_2 molecules in Langevin collision model, and find out the amount of energy exchange between the two particles, we cannot treat it as a one body central-force problem, since we need to assume the two particles are both moving during their interaction period. An example of numerically calculated trajectories of the two particles using classical mechanics is shown in Fig. 4.5 with a specific b and v_0.

If we can perform this calculation for all possible b and v_0, and by accounting the probability of each individual collision event, we can obtain a heating rate caused by background gas collisions. The probability of having a H_2 molecule with speed v_0 can be calculated from Maxwell–Boltzmann speed distribution

$$f(v)\ dv = \left(\frac{m}{2\pi k_B T}\right)^{3/2} 4\pi v^2 e^{-mv^2/(2k_B T)}\ dv, \tag{4.11}$$

where m is the mass of the gas particle, and $f(v)\ dv$ is the probability of the particle having speed between v and $v + dv$. The probability of having a H_2 molecule with impact parameter b can be calculated by modifying the Langevin collision rate.

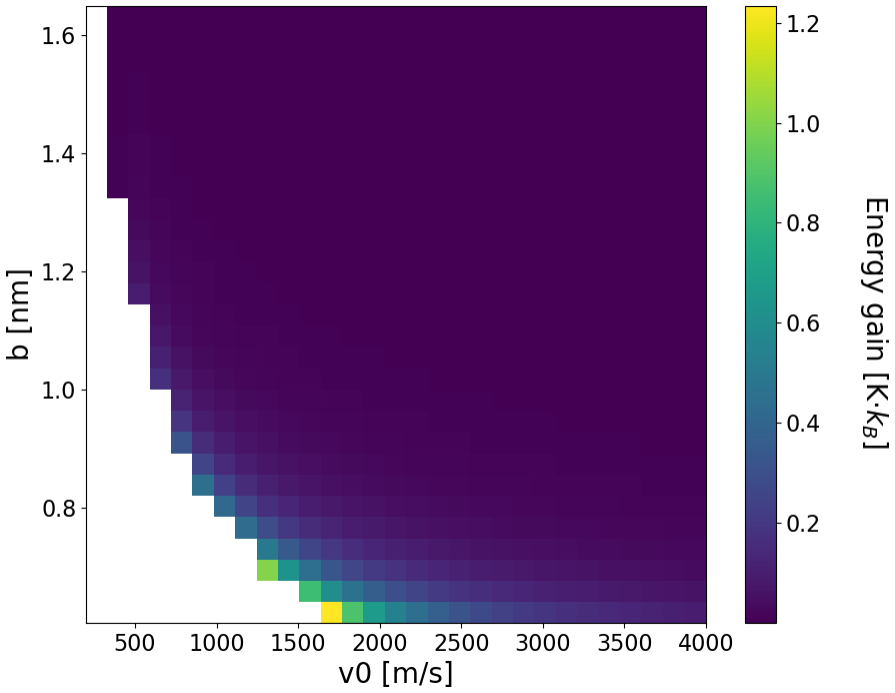

Figure 4.6: **Kinetic energy gain of $^{171}Yb^+$ by colliding with H_2 molecules.** The numerical calculation takes the Yb^+ ion and H_2 in Fig. 4.5, with different impact parameters b and initial speed v_0. The white region refers to the cases with $b < 1.1\, b_{\text{crit}}$, which we did not calculate.

In Fig. 4.6, we show the kinetic energy gain of $^{171}Yb^+$ ion by colliding or interacting with H_2 molecules for all possible collision scenarios, without including the probability of the collision events. We can use this to calculate the heating rate caused by background gas collisions, but the figure shows despite few collision scenarios where $^{171}Yb^+$ ion receives a large amount of energy, most of the collisions are associated with much smaller energy exchange. We do not want the low probability but high energy exchanging collisions to contaminate our heating rate calculation, since their amount of energy exchange is larger than the optical cavity trap depth. We will filter out the collision events with energy exchange larger than the total trap depth. By accounting the probability of each collision

event, and considering the vacuum chamber has pressure of 10^{-9} Pa $= 10^{-11}$ mbar and temperature of 300 K, we find the heating rate caused by background gas collisions is 0.013 mK/s = 46.8 mK/hour per ion, for 50 mK $\cdot\, k_B$ trap depth, and 0.022 mK/s = 79.2 mK/hour per ion, for 100 mK $\cdot\, k_B$ trap depth. This is the heating rate caused by background gas collisions for a single ion, therefore if we have N ions, we should multiply this heating rate by N. The heating rate is also proportional to pressure inside vacuum chamber, and it illustrates the importance of keeping a low pressure.

The value of this heating rate is much larger than recoil heating rate, but it is still much smaller than the trap depth, if we are aiming for a lifetime around few microseconds to few seconds. The high energy collisions can knock the ions out of the trap, but the probability for the collision to occur is extremely low during the lifetime we are considering. For the pressure and temperature we choose to study, Langevin collision rate is 1.3 collisions per hour, and the high energy collision rate is having similar order of magnitude to this Langevin collision rate.

It is worth to note that our method of calculating of heating rate caused by background gas collisions can also be applied to convention ion traps. In convention ion traps, the trap depth is normally much higher than the total kinetic energy of H_2 molecules, and trapping lifetime is much longer than optical trapping, which is measure in unit of hours, therefore we do not need to filter out high energy collision events. For 10^{-9} Pa $= 10^{-11}$ mbar pressure and 300 K temperature, heating rate caused by background gas collisions is 0.086 mk/s = 310 mk/hour plus the heating caused by Langevin collisions. The heating rate cause by low energy collisions is negligible compared to the trap depth and trapping lifetime of conventional ion traps, hence it indicates high energy collision, such as Langecin collisions, are more significant for conventional ion traps.

4.2.2 Changing Optical Potential

In optical cavity trap, the optical potential is offered by AC Stark shift of the ions, and AC Stark shift depends on the laser intensity as shown in Eq. (2.26). Cavity length fluctuation can change the local intensity at the positions of ions, therefore both cavity length and intensity fluctuation introduce noises to the optical potential which can potentially heat up ion the N-ion system. However this heating caused by intensity fluctuation is not a fundamental limitation of optical cavity traps, since it can be minimized by utilizing better experimental procedures and better devices. The fundamental limitation comes from the changing optical potential caused by scattering events of ions.

Since AC Stark shift is a internal state dependent energy shift, if the ion leave ground

internal state, its AC Stark shift will be changed according to which excited state it transits to. If AC Stark shift for an ion in ground internal state is negative providing a trapping potential, the AC Stark shift for the ion in any excited internal state will be positive providing an anti-trapping potential. This conclusion can be derived by using the trace of Hamiltonian matrix is invariant under unitary transformation. Once an ion reach an excited state, it will stay in the excited state for a short duration and emit a photon to decay back to ground state. If this duration, or call it atomic level lifetime, is long enough, the ion can escape the trap, otherwise it will be heated up.

We know for $P_{1/2}$ state of $^{171}\mathrm{Yb}^{+}$, its atomic lifetime is 8 ns. We consider for each scattering event, the ion is exposed in an anti-trapping potential for 8 ns with some initial energy, and find its increase of energy for each scattering event. Considering the optical anti-trapping frequency is $2\times(2\pi\cdot\mathrm{MHz})$, and DC anti-trapping frequency is $0.5\times(2\pi\cdot\mathrm{MHz})$, such that the total anti-trapping frequency is $2.06 \times (2\pi \cdot \mathrm{MHz})$. We can consider the optical anti-trapping frequency to be smaller than optical trapping frequency, since the ground state AC Stark shift is sum of energy shifts from all relevant excited states. The initial position and speed along z direction is determined by its initial energy, and we are assuming the ion only have z direction initial speed, since the anti-trapping potential is only along z direction.

From our calculation, using the anti-trapping frequency of $2.06 \times (2\pi \cdot \mathrm{MHz})$, we find the increase of ion's energy from one scattering event is proportional to its initial energy with a slope of 0.0047. This mean for ion with 1 $\mathrm{mK} \cdot k_B$ initial energy, one scattering event will increase its energy by 0.0047 $\mathrm{mK} \cdot k_B$, similarly, for 100 $\mathrm{mK} \cdot k_B$ initial energy, one scattering event will increase its energy by 0.47 $\mathrm{mK} \cdot k_B$. This is energy increase from one scattering event of each ion. If we consider we have scattering rate of 10 s^{-1}, and we are trapping 10 ions, the heating rate per second must be higher than 100 times the temperature increase from each scattering event. If we multiply the results by 100, the increase of system's temperature in one second of this heating rate is comparable to optical cavity trap depth. Based on our analysis of other sources of heating rate, we think heating rate caused by scattering is fundamentally limiting the lifetime of optical cavity trap.

Since the energy increase of each ion depends on its initial energy, and each scattering event will increase its energy, the heating rate for each ion should not be multiplying the energy increase by scattering rate. The heating rate should be higher than that. However, since the slope $0.0047 \ll 1$ is much less than 1, if we perform the calculation by considering each scattering event changes the initial energy of next event, and after 10 scattering events, the heating rate is not much different from the heating rate obtained by multiplying energy increase with scattering rate.

4.2.3 Conclusion for Lifetime and Scalability

By estimating the heating rate from different sources, we find the heating rate caused by scattering is much larger than background gas collisions, which is also much larger than recoil heating rate. We think without considering the environmental fluctuations, i.e stray electric field fluctuation and cavity intensity fluctuation, the dominant source of heating rate is photon scattering from ions. In addition, the scattering rate is proportional to intensity, such that we cannot mitigate heating effect by increasing our optical cavity trap depth. The heating rate from scattering is proportional to both initial energy of the ion and scattering rate, it should be positively correlated with the number of ions in the trap. Note that we do not know how to connect single ion heating rate to multi-ion heating rate, therefore we cannot predict how trapping lifetime scale with N. But let's try to think about this question by looking at each individual ion.

Recall in Section 4.2, we define trapping probability of N ions is the probability for any one of the N ions does not escape the trap. Trapping lifetime is the time for trapping probability of N ions to reach $1/e$. Therefore if we wish to trap N ions, the trapping probability for each ion at the end of trapping lifetime should be $(1/e)^{1/N}$, e.g. for $N = 20$, $(1/e)^{1/N} = 0.95$. We see that trapping lifetime for N ions should be much smaller than the lifetime for one ion.

Consider the case of trapping 20 $^{171}Yb^{+}$ ions in 2D structure in optical cavity trap, each ion has initial energy of ~ 1 mK $\cdot\, k_B$ with ~ 100 mK $\cdot\, k_B$ trap depth provide by 1064 nm laser, we will have scattering rate to be around ~ 30 s^{-1} for each ion. If we can assume single ion trapping probability is $\sim (1 - E/V_{\text{depth}})$, where E is the energy of the single ion. Based on our previous heating rate analysis, we have trapping lifetime for $N = 20$ ions of ~ 35 s. However, this trapping lifetime is too longer to be true.

Recall again in Section 2.5, we mention for each scattering event of Yb^{+}, there is a 5% probability for the ion to scatter to meta-stable D manifold. If we are considering a total scattering rate as ~ 30 s^{-1} for each ion, the scattering rate to meta-stable D manifold is ~ 0.15 s^{-1} for each ion. The states in D manifold are anti-trapping states under 1064 nm, and once the ion reach this manifold, it cannot go back to the ground state directly, therefore we can consider the ion is lost once it decays to this manifold. This strongly limits the trapping lifetime of systems with multiple ions. Assuming scattering to meta-stable states is the only lose mechanism, the trapping probability for each ion is $e^{-0.15t}$, where 0.15 is the scattering rate to meta-stable states, and t has unit of second. Since for $N = 20$ ions, trapping lifetime is the time for trapping probability for each ion to decay to $(1/e)^{1/N} = 0.95$, we have trapping lifetime of $t = 0.342$ s $= 342$ ms, such that $e^{-0.15t} = 0.95$. For $N = 10$ ions, trapping lifetime is the time for trapping probability for

each ion to decay to $(1/e)^{1/N} = 0.90$, the trapping lifetime becomes $t = 702$ ms, if the scattering rate is unchanged. We find the scattering to meta-stable states for large N is more problematic.

We eventually find the lose mechanism of ions of large N is not governed by temperature increase of the system, but by scattering probability to meta-stable D manifold. However, we cannot reach this conclusion without having the previous heating rate analysis. In the case of large N, we now know how trapping lifetime scales with N, which is scaled by $1 - (1/e)^{1/N}$. Trapping lifetime does not necessarily determine coherence time of the quantum states, since coherence time is mostly limited by total scattering rate in optical traps, which will be discussed in next chapter.

Chapter 5

Conclusion and Outlook

We introduce the basic concepts and mechanisms for optical ion trapping in this thesis, which is providing theoretical supports to our study of 2D ion trapping. We propose a scheme to trap 2D ion crystals with optical cavity trap. We develop systemic methods to study the structural and mechanical properties of 2D ion crystals with the presence of optical cavity trap potential. This study helps us to find sets of experimental feasible trapping parameters for optical cavity ion trap with different ion number N. We provide stability analysis and trapping lifetime estimation for 2D ion crystals in optical cavity trap. We study lifetime by first estimating the heating rate of the system from different sources, to get a sense of how they affect the system. The heating rate estimation can help us to estimate trapping lifetime for small N, but for large N, we find the trapping lifetime is fundamentally limited by scattering rate to meta-stable D manifold of the ion. We thus find how trapping lifetime scales with N for large N.

Some of our results not only apply to optical traps but also conventional traps, e.g. potential barrier analysis between different equilibrium positions of 2D ion crystals, and heating rate caused by background gas collisions. Some of our results seems to be redundant, e.g. we find heating rate caused by background gas collisions is too small to change trapping lifetime, but we do not know the significance before getting the final result.

We mention both red and blue detuned lasers can be used to trap ions, but we only work with red detuned lasers. The analysis for trapping parameters and lifetime for blue detuned lasers is very different from red detuned lasers. Blue detuned lasers normally have smaller laser power than red detuned ones such that we need to choose a smaller laser detuning to create enough AC Stark shift, but this makes the scattering rate to be high. As discussed in Section 3.2.3, ions are trapped at zero intensity plane with blue detuned lasers. If

the trapped ions have zero temperature, they will not scatter photons, since the local laser intensity at ions' positions is zero. However, ions cannot be initialized at zero temperature, and their kinetic energy can deviate them from the zero intensity plane. The scatter rate will not be zero, and the scattering events will continuously increase its temperature. Since the scattering rate can be suppressed by having a low initial temperature, we may expect optical ion trapping with blue detuned lasers to have brighter potential for scalability and longer quantum coherence times, which can be explored in future studies.

To discuss whether a trapped ion system is capable of performing QIP experiments, we need to estimate the time scales for quantum gate time and the available quantum coherence time from the trap. Quantum logic gates consist of a sequence of single and two-qubit operations. Normally, single-qubit operations are several orders of magnitude faster than two-qubit operations, therefore quantum gate time is determined by the time required for two qubits operations. For example, the Mølmer–Sørensen scheme [2, 3] to perform two-qubit operations, the required time is of the order of ~ 1 ms [17]. The coherence times estimation for conventional and optical traps are very different. The coherence times of optical traps are fundamentally limited by scattering rate, e.g. when performing a two-qubit gate, we do not want both of the two ions to scatter photons during the gate time. Again, considering each ion has scattering rate of 30 s^{-1}, the time for the probability of both of the two ions do not scatter to reach 90% is 1.8 ms. The estimated coherence time and Mølmer–Sørensen gate time are having similar order of magnitude, which means it is difficult to apply a sequence of Mølmer–Sørensen gates during coherence time. It is possible to make Mølmer–Sørensen gate time shorter by increasing the axial trap frequency, and it is also possible to make coherence time to be longer by reducing scattering rate, e.g. scattering rate can be reduced by reducing ion number N, since the required trap frequency and laser intensity will be smaller. However, it is hard to make orders of magnitude changes to the numbers, thus we think it is challenging to perform QIP experiments using Mølmer–Sørensen gates in optical ion traps with red detuned lasers. One potential solution is using faster gates [18] than Mølmer–Sørensen gates, and another approach is investigating optical ion traps with blue detuned lasers, since it can potentially provides us with a low scattering rate period after initializing the system at a low temperature.

References

[1] J. I. Cirac and P. Zoller. Quantum computations with cold trapped ions. *Phys. Rev. Lett.*, 74:4091–4094, May 1995.

[2] Klaus Mølmer and Anders Sørensen. Multiparticle entanglement of hot trapped ions. *Phys. Rev. Lett.*, 82:1835–1838, Mar 1999.

[3] Anders Sørensen and Klaus Mølmer. Quantum computation with ions in thermal motion. *Phys. Rev. Lett.*, 82:1971–1974, Mar 1999.

[4] Adriano Barenco, Charles H. Bennett, Richard Cleve, David P. DiVincenzo, Norman Margolus, Peter Shor, Tycho Sleator, John A. Smolin, and Harald Weinfurter. Elementary gates for quantum computation. *Phys. Rev. A*, 52:3457–3467, Nov 1995.

[5] Wolfgang Paul. Electromagnetic traps for charged and neutral particles. *Rev. Mod. Phys.*, 62:531–540, Jul 1990.

[6] Marissa D'Onofrio, Yuanheng Xie, A. J. Rasmusson, Evangeline Wolanski, Jiafeng Cui, and Philip Richerme. Radial two-dimensional ion crystals in a linear paul trap. *Phys. Rev. Lett.*, 127:020503, Jul 2021.

[7] Alexander Lambrecht, Julian Schmidt, Pascal Weckesser, Markus Debatin, Leon Karpa, and Tobias Schaetz. Long lifetimes and effective isolation of ions in optical and electrostatic traps. *Nature Photonics*, 11(11):704–707, Nov 2017.

[8] Ch. Schneider, M. Enderlein, T. Huber, and T. Schaetz. Optical trapping of an ion. *Nature Photonics*, 4(11):772–775, Nov 2010.

[9] Julian Schmidt, Alexander Lambrecht, Pascal Weckesser, Markus Debatin, Leon Karpa, and Tobias Schaetz. Optical trapping of ion coulomb crystals. *Phys. Rev. X*, 8:021028, May 2018.

[10] Rudolf Grimm, Matthias Weidemüller, and Yurii B. Ovchinnikov. Optical dipole traps for neutral atoms. volume 42 of *Advances In Atomic, Molecular, and Optical Physics*, pages 95–170. Academic Press, 2000.

[11] Harold J. Metcalf and Peter van der Straten. Laser cooling and trapping. Springer Science, Business Media New York, 1999.

[12] Christian Schneider, Martin Enderlein, Thomas Huber, Stephan Dürr, and Tobias Schaetz. Influence of static electric fields on an optical ion trap. *Phys. Rev. A*, 85:013422, Jan 2012.

[13] Ye Wang, Mu Qiao, Zhengyang Cai, Kuan Zhang, Naijun Jin, Pengfei Wang, Wentao Chen, Chunyang Luan, Botao Du, Haiyan Wang, and et al. Realization of two-dimensional crystal of ions in a monolithic paul trap. *Advanced Quantum Technologies*, 3(11):2000068, Oct 2020.

[14] Daniel H. E. Dubin. Theory of structural phase transitions in a trapped coulomb crystal. *Phys. Rev. Lett.*, 71:2753–2756, Oct 1993.

[15] J. P. Schiffer. Phase transitions in anisotropically confined ionic crystals. *Phys. Rev. Lett.*, 70:818–821, Feb 1993.

[16] D. J. Wineland, C. Monroe, W. M. Itano, D. Leibfried, B. E. King, and D. M. Meekhof. Experimental issues in coherent quantum-state manipulation of trapped atomic ions. *Journal of Research of the National Institute of Standards and Technology*, 103:259–328, May-Jun 1998.

[17] C. Monroe, W. C. Campbell, L.-M. Duan, Z.-X. Gong, A. V. Gorshkov, P. W. Hess, R. Islam, K. Kim, N. M. Linke, G. Pagano, P. Richerme, C. Senko, and N. Y. Yao. Programmable quantum simulations of spin systems with trapped ions. *Rev. Mod. Phys.*, 93:025001, Apr 2021.

[18] V. M. Schäfer, C. J. Ballance, K. Thirumalai, L. J. Stephenson, T. G. Ballance, A. M. Steane, and D. M. Lucas. Fast quantum logic gates with trapped-ion qubits. *Nature*, 555:75–78, Mar 2018.

APPENDICES

Appendix A

Atomic Energy Levels Diagram

A.1 Yb^+ Energy Levels Diagram

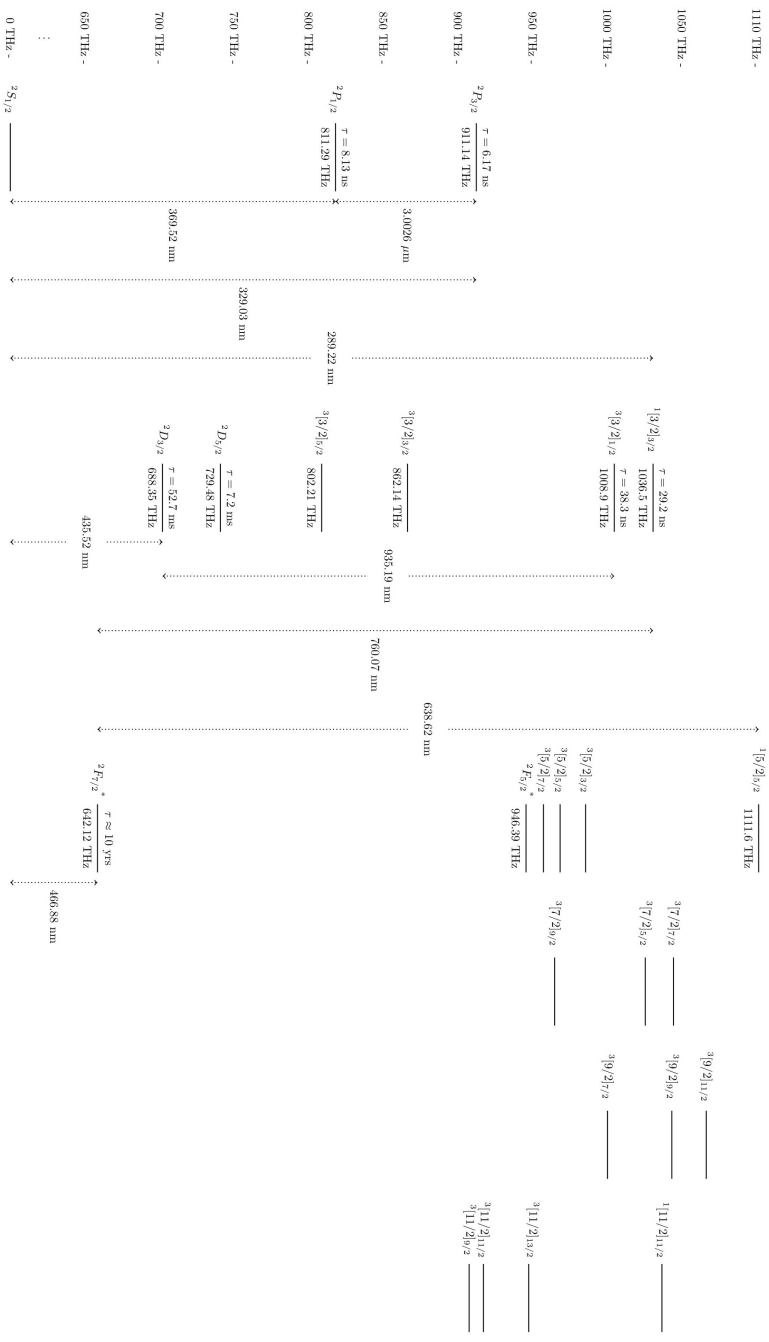

Figure A.1: **Yb^+ fine energy levels diagram.** Brackets states are using J_1K coupling notation. The plot is scaled by the energy difference between states.

A.2 $^{171}Yb^{+}$ Hyperfine Levels Diagram

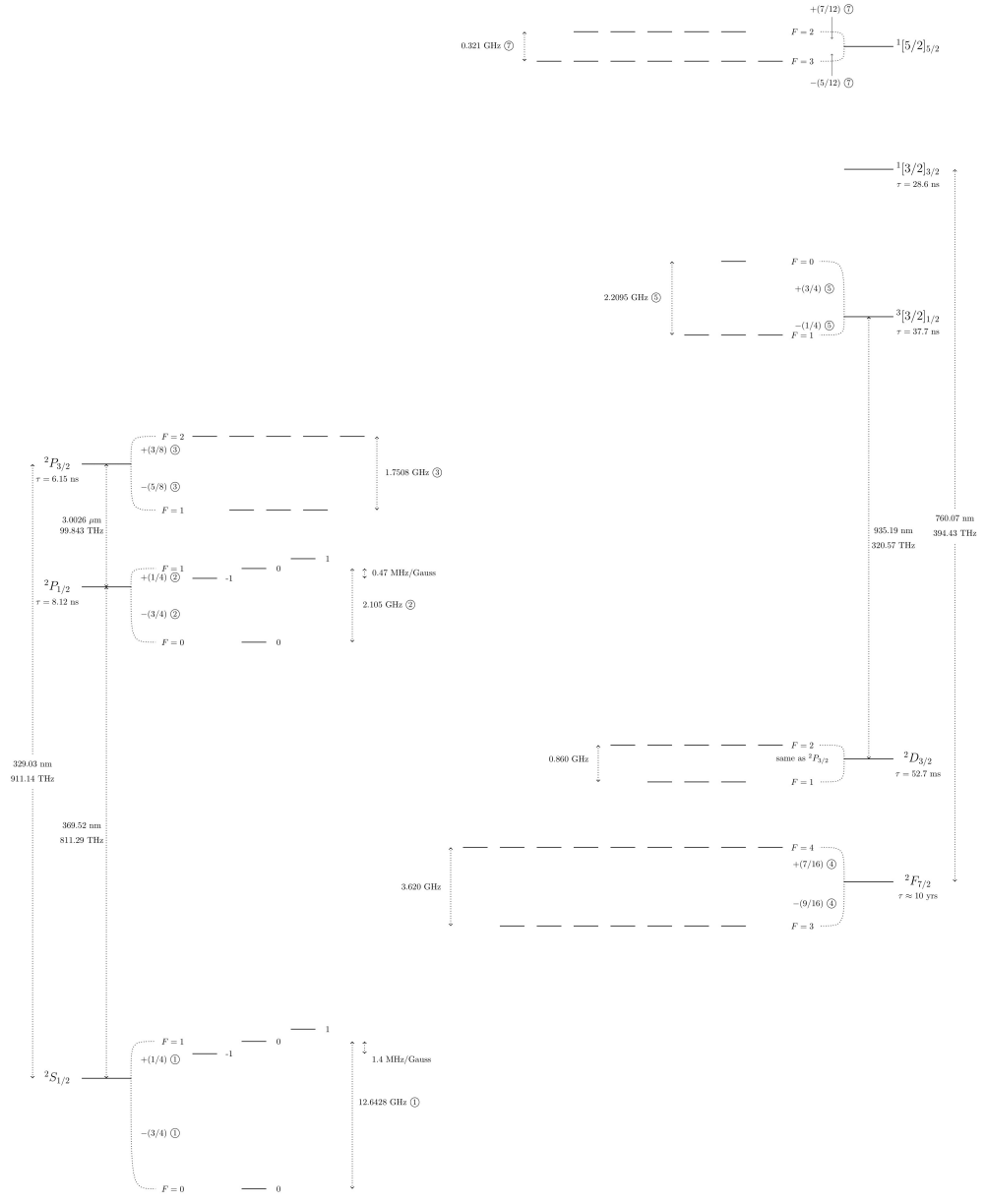

Figure A.2: **Yb^{+} fine energy levels diagram.** Brackets states are using J_1K coupling notation. The plot is scaled by the energy difference between states.

Appendix B

Conventional to Optical Trapping Adiabatic Transfer

Before any QIP experiment, the quantum systems must be initialized into the desire qubit state, and after the experiment, we also need to detect the final state of the system. For QIP experiments with trapped ion system, performing initialization and detection on each ion requires the ion to scatter photons. Normally, from an order of magnitude estimation, state initialization takes ~ 10 scattering events to complete, and detection requires ~ 1000 scattering events. From Section 4.2.2, we know scattering events limit the optical trapping lifetime, therefore we wish to move initialization and detection stages out of optical trapping period.

The optical trapping period is sandwiched with conventional trapping, and transferring the system between conventional and optical trapping is associated with ramping up or down optical and RF trapping potentials. Internal states of ions are stable against changing trapping potentials, but external (motional) states are not. Changing trapping potential in time can heat up the system such that the external state of the system is changed. Adiabatic transfer refers to the transferring process which is slow enough such that external state of the system in unchanged after the process. However, we cannot make the process to be arbitrarily long, since it must be much shorter than optical trapping lifetime. We thus need to optimize the rate of ramping up or down optical and RF trapping potentials.

It is easy to move detection stage out of optical trapping period, since the QIP experiment is complete before the detection stage, and we do not care about external states anymore. For each ion, after the very first scattering event in detection stage, its quantum state collapse into one of the qubit states, which is normally chosen as the hyoerfine levels

of ground internal states. At this point, we do not need adiabatic transferring.

As for initialization stage, we do care about the external state of the system. Our task is to calculate the optimized ramping rate of optical and RF trapping potentials during conventional to optical trapping transferring process, such that the propagator of initial and final external states of the system is maximized. Consider a simple case where we first ramp up optical cavity potential from t_0 to t_1, then start to ramp down conventional potential from t_1 to t_2. We have

$$V_{\text{tot}}(t) = \lambda_{\text{opt.}}(t)V_{\text{opt.}} + V_{\text{con.}},\ t_0 < t < t_1, \tag{B.1}$$

$$V_{\text{tot}}(t) = V_{\text{opt.}} + \lambda_{\text{con.}}(t)V_{\text{con.}},\ t_1 < t < t_2, \tag{B.2}$$

and

$$\lambda_{\text{opt.}}(t),\ \lambda_{\text{con.}}(t) \in [0, 1], \tag{B.3}$$

where $\lambda_{\text{opt.}}(t)$ and $\lambda_{\text{con.}}(t)$ are the ramping rates for optical cavity and conventional trapping potentials. The ramping rate $\lambda_{\text{opt.}}(t)$ is increasing in time, and $\lambda_{\text{con.}}(t)$ is decreasing in time. We are trying to find the $\lambda_{\text{opt.}}(t)$ and $\lambda_{\text{opt.}}(t)$ such that $\langle\psi(t_0)|\psi(t_2)\rangle$ is maximized, where $|\psi(t)\rangle$ is the external state of the system.

By dividing the time interval $[t_0, t_1]$ into many smaller dt intervals and applying time dependent perturbation theory, we can calculate $\langle\psi(t)|\psi(t+dt)\rangle$ for a given $d\lambda/dt$ within this interval dt. Numerically performing this calculation iteratively, we can find the relation between $\lambda(t)$ and $\langle\psi(t_0)|\psi(t_2)\rangle$. Now we need an optimization algorithm to complete our task. We can make use of the optimization algorithm which we used to calculate the optimized path between different equilibrium positions of ion crystals in Section 4.1, by treating $\lambda(t)$ as the path of N-ion position, and $\langle\psi(t)|\psi(t+dt)\rangle$ as the potential energy of N-ion position. This approach can be generalized to more complicated cases. If we want to ramp optical and conventional trapping potentials at the same time, we only need to optimize an array of $[\lambda_{\text{opt.}}(t), \lambda_{\text{con.}}(t)]$ with respect to $\langle\psi(t_0)|\psi(t_f)\rangle$, where t_f is the final time.